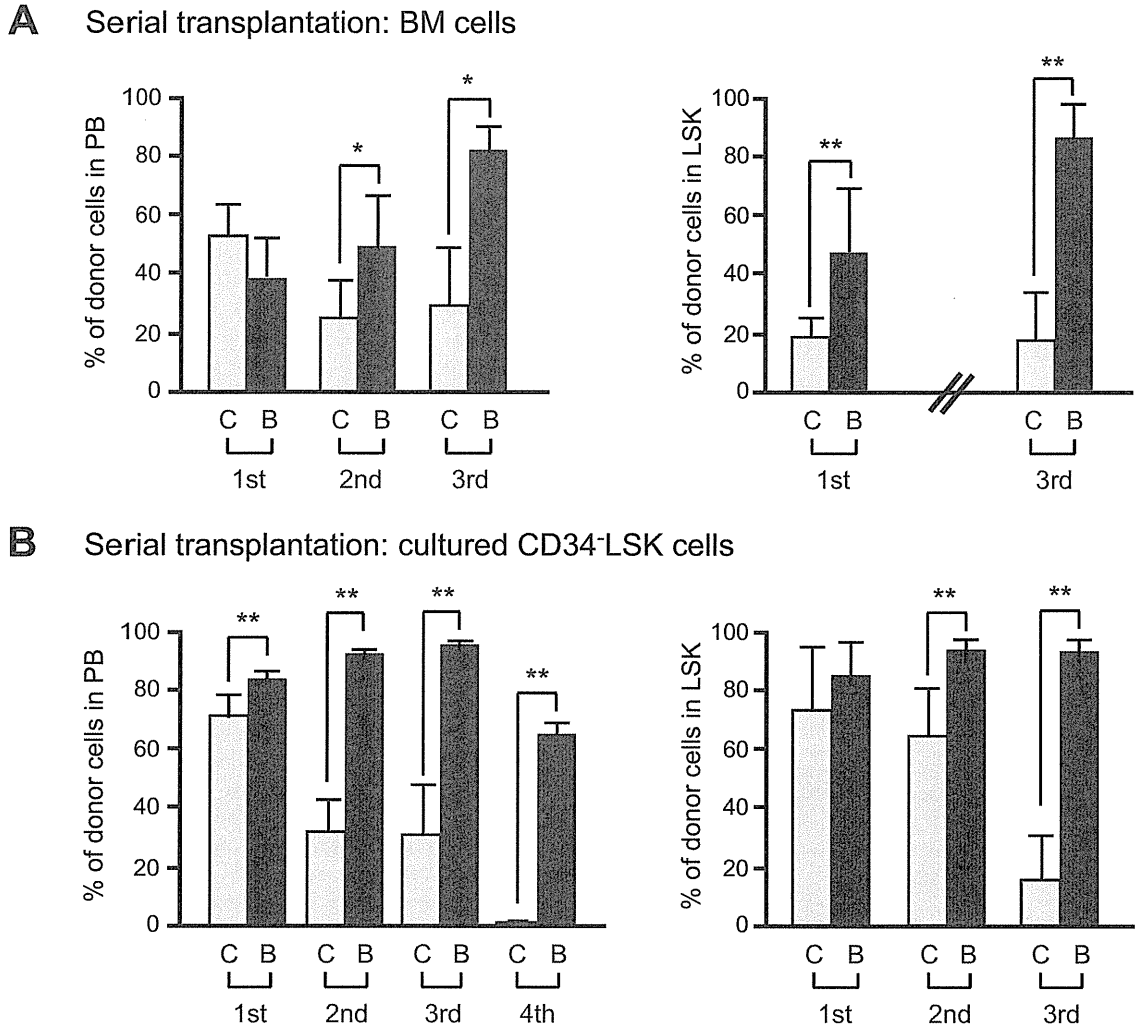


**Figure 4. Overexpression of *Bmi1* protects HSCs during serial transplantation.** (A) Serial transplantation of BM cells. BM cells ($5\times10^5$) from *Tie2-Cre* (denoted as "C") and *Tie2-Cre;R26Stop$^{FL}$Bmi1* (denoted as "B") mice (CD45.2) along with $5\times10^5$ competitor BM cells (CD45.2) were transplanted into CD45.1 recipient mice lethally irradiated at a dose of 9.5 Gy. For serial transplantation, BM cells were collected from all recipient mice at 12–20 weeks after transplantation and pooled together. Then, $5\times10^6$ BM cells were transplanted into lethally irradiated recipient mice without competitor cells. Third and fourth transplantation were similarly performed using $5\times10^6$ pooled BM cells. Percent chimerism of donor cells in the recipient PB and BM LSK cells was determined at 16 weeks post-transplantation. Results are shown as the mean ± S.D. (n = 6, 3$^{rd}$ transplantation; n = 4). (B) Serial transplantation of cultured CD34$^-$LSK cells. CD34$^-$LSK cells were cultured in the SF-O3 serum-free medium supplemented with 50 ng/ml of SCF and TPO for 10 days. Then, the cells in culture corresponding to the 20 initial CD34$^-$LSK cells were injected into a recipient mouse along with $2\times10^5$ competitor BM cells (CD45.2) as described in (A) (n = 6, 4$^{th}$ transplantation; n = 5). * $P<0.05$, ** $P<0.01$.
doi:10.1371/journal.pone.0036209.g004

## Overexpression of *Bmi1* has no Impact on Radioprotection

DNA damage is intimately linked to stem cell aging. Heritable DNA damage accrued in stem cells leads to stem cell senescence or apoptosis, which over time can lead to the depletion of the stem cell pool and reduced regenerative capacity of stem cells [18]. Bmi1 is rapidly recruited to sites of DNA damage and is required for DNA damage-induced ubiquitination of histone H2A at lysine 119. Loss of Bmi1 leads to impaired repair of DNA double-strand breaks (DSBs) by homologous recombination [19,20]. In glioblastoma multiforme (GBM) cells, Bmi1 was co-purified with DSB response proteins, such as ATM and the histone γH2AX, and non-homologous end joining (NHEJ) repair proteins. Of interest, BMI1 overexpression in normal neural stem cells enhanced ATM recruitment to the chromatin, the rate of γH2AX foci resolution, and resistance to radiation [21]. In order to understand the role of overexpressed Bmi1 in HSCs, we examined the radioresistance of HSCs by quantifying the number of γH2AX foci following genotoxic stress, a metric which reflects DNA DSBs.

We purified CD34$^-$LSK cells from *Tie2-Cre* and *Tie2-Cre;R26-Stop$^{FL}$Bmi1* mice and irradiated them at a dose of 2 Gy. At 2 and 4 hours after irradiation, cells were stained with anti-γH2AX. We expected rapid resolution of γH2AX by overexpression of *Bmi1*, but no significant difference was observed in the number of γH2AX foci between *Tie2-Cre* and *Tie2-Cre;R26Stop$^{FL}$Bmi1* HSCs (**Figure 5A**). HSCs recovered from the recipients of tertiary transplantation did not show any difference in the number of γH2AX foci, either (**Figure 5B**). We then tested hematopoietic recovery after irradiation in mice. We irradiated recipient mice reconstituted with *Tie2-Cre* and *Tie2-Cre;R26Stop$^{FL}$Bmi1* BM cells at a dose of 5 Gy, and monitored hematopoietic recovery for 4 weeks. The recovery of hematopoietic components in PB as well as

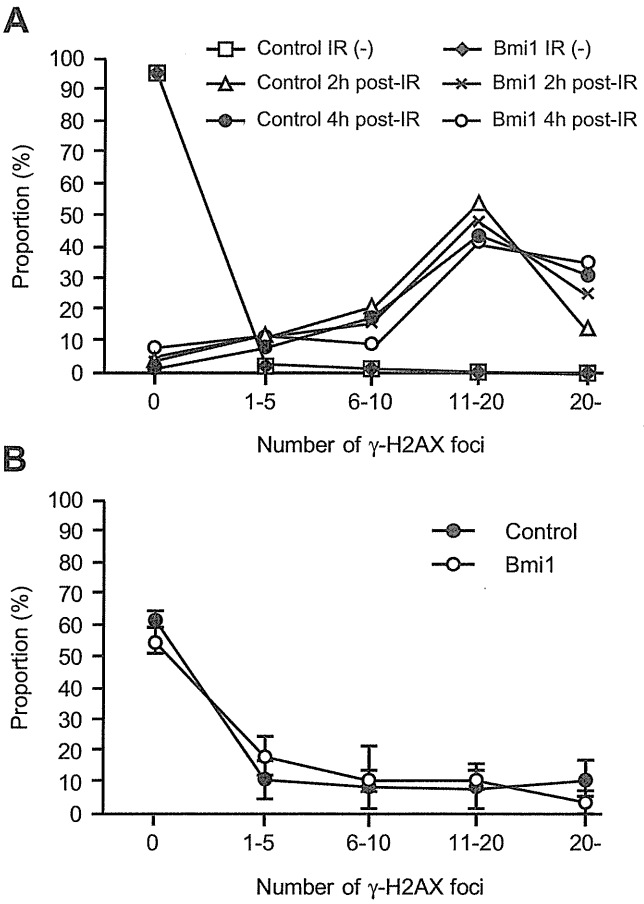


**Figure 5. DNA damage response of *Tie2-Cre;R26Stop$^{FL}$Bmi1* HSCs.** (A) DNA damage response of CD34$^-$LSK cells from *Tie2-Cre* (Control) and *Tie2-Cre;R26Stop$^{FL}$Bmi1* (Bmi1) mice *in vitro*. Purified CD34$^-$LSK cells were irradiated (IR) at a dose of 2 Gy. At 2 and 4 hours after irradiation, cells were stained with anti-γH2AX. Numbers of γH2AX foci expressed per cell are depicted. (B) DNA damage response of CD34$^-$LSK cells from *Tie2-Cre* (Control) and *Tie2-Cre;R26Stop$^{FL}$Bmi1* (Bmi1) mice *in vivo*. LSK cells were purified from the recipients of tertiary transplantation and stained with anti-γH2AX. Numbers of γH2AX foci expressed per cell are depicted as the mean ± S.D. (n = 3).
doi:10.1371/journal.pone.0036209.g005

BM LSK cells was comparable between the two groups (**Figure S3**). These findings suggest that overexpression of *Bmi1* does not afford an advantage to HSCs in their ability to resist genotoxic stress.

## Overexpression of *Bmi1* Confers Resistance to Oxidative Stress on HSCs

HSCs contain lower levels of reactive oxygen species (ROS) than their mature progeny in order to maintain their quiescent state. ROS reportedly act through p38 mitogen-activated protein kinase (MAPK) to limit the lifespan of HSCs [16,22]. It has been demonstrated that prolonged treatment with the antioxidant *N*-acetyl-$_L$-cysteine (NAC) or an inhibitor of p38 MAPK extends the lifespan of HSCs in serial transplantation assays, suggesting that oxidative stress is one of the major factors that affects HSC function during these assays [16,17,23]. Given that *Tie2-Cre;R26-Stop$^{FL}$Bmi1* HSCs retain self-renewal capacity during serial transplantation, overexpression of *Bmi1* may bestow a protective effect onto HSCs against oxidative stress.

To address this question, we cultured HSCs in the presence of buthionine sulfoximine (BSO), which depletes intracellular glutathione and thereby increases intracellular ROS levels. We found that highly purified CD34$^-$LSK HSCs were susceptible to an increase in ROS levels because treatment with BSO significantly suppressed their growth and induced cell death (data not shown). After 3 days of BSO treatment, surviving cells were subjected to colony-forming assays. Both *Tie2-Cre* control and *Tie2-Cre;R26-Stop$^{FL}$Bmi1* HSCs cultured with BSO gave rise to significantly fewer colonies than HSCs cultured without BSO. Interestingly, *Tie2-Cre;R26Stop$^{FL}$Bmi1* HSCs gave rise to a significantly more colonies than the control HSCs (**Figure 6A**). Notably, the number of HPP colonies was reduced 48-fold after treatment of control HSCs with BSO, but only 3-fold upon overexpression of *Bmi1*. The frequency of CFU-nmEM was also less perturbed following treatment with BSO in HSCs overexpressing *Bmi1*. These results indicate a role for Bmi1 in the resistance to oxidative stress.

Bmi1 regulates mitochondrial function by regulating the expression of a cohort of genes related to mitochondrial function and ROS generation. *Bmi1*-deficient cells have impaired mitochondrial function, which causes a marked increase in the intracellular levels of ROS [24]. Based on these observations, we then measured the intracellular ROS levels in CD34$^-$LSK cells at day 14 of culture. Unexpectedly, overexpression of *Bmi1* did not affect the levels of ROS in either LSK HSCs/MPPs or Lin$^-$Sca-1$^{low/-}$c-Kit$^+$ downstream progenitors (**Figure 6B**). Overexpression of *Bmi1* had no significant effect on the ROS levels even in the presence of BSO (**Figure S4**). Likewise, treatment of cells with the antioxidant NAC promoted cell growth and increased the proportion of LSK cells in both control and *Tie2-Cre;R26-Stop$^{FL}$Bmi1* culture similarly (**Figure 6C** and data not shown). These results indicate that an excess of Bmi1 does not regulate the generation or scavenging of ROS, but confers resistance to higher levels of ROS on HSCs through unknown mechanisms.

## Discussion

In this study, we generated a new mouse line where *Bmi1* can be conditionally overexpressed in a hematopoietic cell-specific fashion and analyzed the effect of overexpression of *Bmi1* in detail. Overexpression of *Bmi1* did not significantly affect steady state hematopoiesis, but it efficiently protected HSCs from stresses. Our findings suggest that overexpression of *Bmi1* confers resistance to stresses on HSCs, thereby augmenting their regenerative capacity.

Recent findings have established that the regulation of oxidative stress in HSCs is critical for the maintenance of HSCs. In this study, we demonstrated that overexpression of *Bmi1* protects HSCs from loss of self-renewal capacity at least in part by increasing the capacity of HSCs to resist oxidative stress. It has been reported that *Bmi1*-deficient mice have an increased level of intracellular ROS due to de-regulated expression of genes related to mitochondrial function and ROS generation [24,25]. However, an excess of Bmi1 in this study had no effect on the levels of intracellular ROS. Thus, it is hypothesized that Bmi1 is negatively regulated downstream of the ROS signal and an excess of Bmi1 overcomes this negative regulation. Indeed, ROS reportedly primes *Drosophila* hematopoietic progenitors for differentiation and this process involves downregulation of PcG activity [26]. ROS signaling activates p38 and eventually releases the transcriptional repression of *p16$^{Ink4a}$* and *p19$^{Arf}$*, critical targets of Bmi1 [16]. Furthermore, recent studies including ours have revealed that PcG proteins are downregulated and dissociate from the *Ink4a/Arf* locus when cells are exposed to intra- or extracellular stress, including tissue culture- and oncogene-induced stress

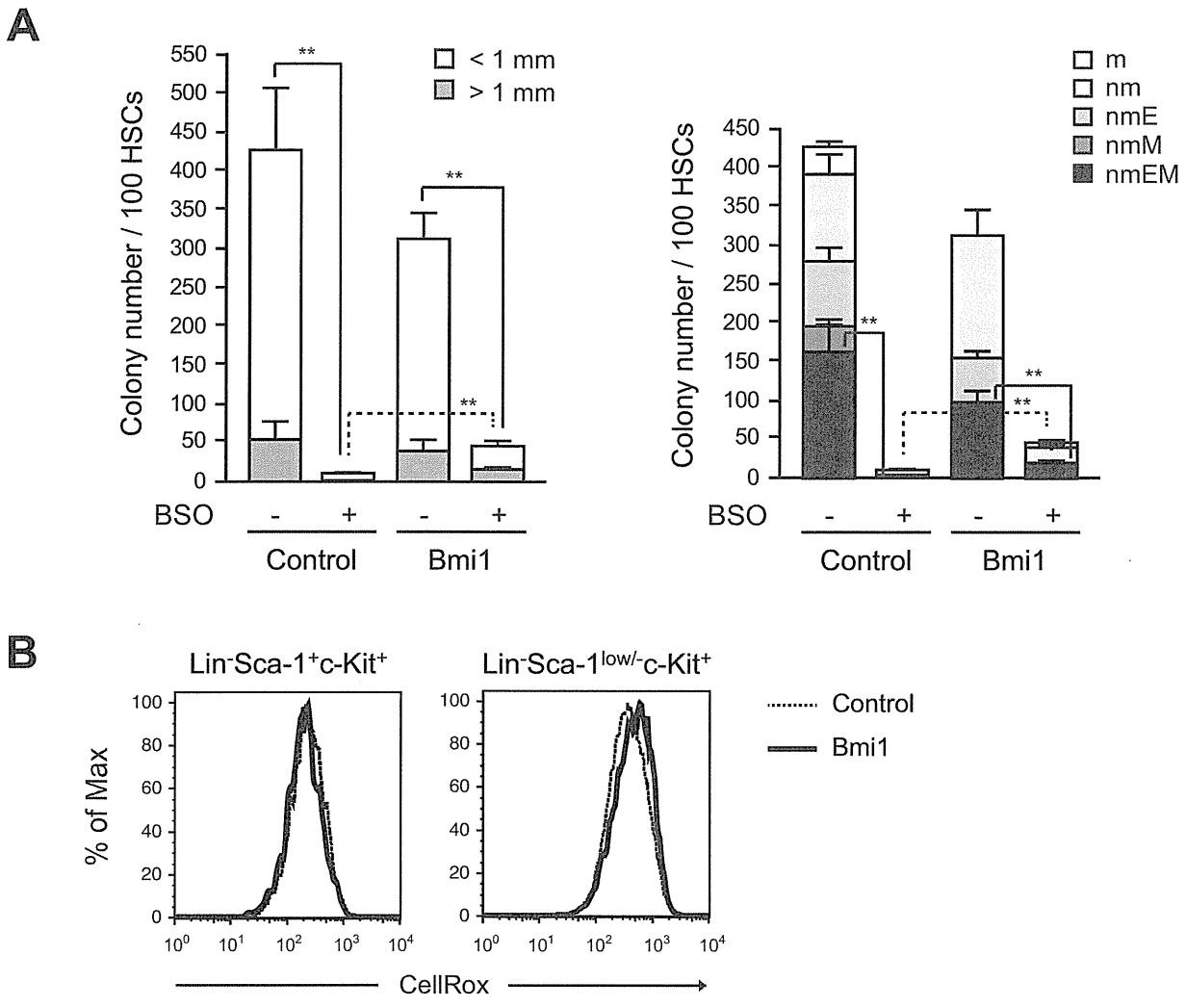
A
Colony number / 100 HSCs
< 1 mm
> 1 mm
m
nm
nmE
nmM
nmEM
BSO
Control
Bmi1
B
Lin-Sca-1+c-Kit+
Lin-Sca-1low/-c-Kit+
% of Max
Control
Bmi1
CellRox
C
Tie2-Cre; NAC(-)
Tie2-Cre;R26StopFLBmi1; NAC(-)
Tie2-Cre; 150 μM NAC
Tie2-Cre;R26StopFLBmi1; 150 μM NAC
Lineage marker
c-Kit
Sca-1
6.82
0.19
24.0
1.24
8.72
0.50
17.6
2.39

**Figure 6. Overexpression of Bmi1 confers oxidative stress on HSCs.** (A) Colony formation by HSCs cultured for 3 days. $CD34^-LSK$ cells from *Tie2-Cre* (Control) and *Tie2-Cre;R26Stop$^{FL}$Bmi1* (Bmi1) mice were cultured in the SF-O3 serum-free medium supplemented with 50 ng/ml SCF, TPO and 0.05 mM of BSO. At day 3 of culture, the cells were plated in methylcellulose medium to allow formation of colonies in the presence of 20 ng/ml SCF, 20 ng/ml TPO, 20 ng/ml IL-3, and 3 u/ml EPO. Absolute numbers of LPP and HPP-CFCs (left panel) are shown as the mean ± S.D. for triplicate cultures. Absolute numbers of each colony types are shown in the right panel. Data are shown as the mean ± S.D. for triplicate analyses. Statistical analyses were performed on the total colony numbers (left panel) and nmEM colony numbers (right panel), respectively. $^{**}p<0.01$. (B) Levels of ROS in cells overexpressing *Bmi1*. $CD34^-LSK$ cells from *Tie2-Cre* (Control) and *Tie2-Cre;R26Stop$^{FL}$Bmi1* (Bmi1) mice were cultured in the SF-O3 serum-free medium supplemented with 50 ng/ml SCF and TPO. Representative flow cytometric profiles of LSK and Lineage marker$^-$Sca-$1^{low/-}$c-$Kit^+$ cells in cultures at day 14 are depicted. (C) Effects of NAC on *Bmi1* culture. $CD34^-LSK$ cells from *Tie2-Cre* and *Tie2-Cre;R26Stop$^{FL}$Bmi1* mice were cultured in the SF-O3 serum-free medium supplemented with 50 ng/ml SCF and TPO in the presence and absence of 150 μM NAC. Representative flow cytometric profiles of LSK cells in cultures at day 14 are depicted. The proportion of $Lin^-$ and LSK cells in total cells are indicated.
doi:10.1371/journal.pone.0036209.g006

[27,28]. Together, this accumulating evidence suggests that Bmi1 is dynamically regulated in response to oxidative stress, probably downstream of p38. Our preliminary data demonstrated that activated p38 directly phosphorylates Bmi1 *in vitro* (Oshima and Iwama., unpublished data). Thus, it is possible that p38, which is activated by oxidative stress, attenuates Bmi1 function via direct phosphorylation of Bmi1. How oxidative stress restricts the expression and function of Bmi1 is an important issue to be addressed.

Of note, the effect of Bmi1 overexpression in serial transplantation resembles that of overexpression of *Ezh2*, a gene encoding a core component of PRC2 [29]. Overexpression of PcG genes, *Bmi1* and *Scmh1*, also induces tolerance of cortical neurons to ischemia [30]. Thus, various cellular stresses may target PcG complexes to release transcriptional repression of PcG-regulated genes, such as tumor suppressor and developmental regulator genes, thereby affecting stemness. All these findings support the notion that enforcement of PcG function is a key for successful regenerative therapies.

Meanwhile, the role of PcG proteins in resistance to oxidative stress is also implicated in cancer. Expression of PcG proteins including *BMI1* and *EZH2* are often up-regulated in various cancers, particularly in their cancer stem cell fractions [31]. Interestingly, cancer stem cells in some tumors appear to be susceptible to ROS, similar to normal stem cells, and thus develop mechanisms to keep the levels of ROS low [32]. Interference of EZH2 function by the small-molecule histone methyltransferases inhibitor, DZNep, is reported to increase ROS levels in acute myeloid leukemia cells like in *Bmi1*-deficient mice [33]. Conversely, our findings in this study suggest that an excess of PcG proteins often observed in aggressive cancer could help cancer stem cells tolerate oxidative stress. In this regard, overexpression of PcG proteins could also be therapeutic targets in cancers including leukemia. Finally, no *Tie2-Cre;R26Stop$^{FL}$Bmi1* mice developed hematological malignancies during the observation period, up to 18 months after birth. Only one recipient mice with *Tie2-Cre;R26Stop$^{FL}$Bmi1* BM cells developed acute lymphocytic leukemia in the tertiary transplantation. These findings suggest that Bmi1 by itself is not sufficient to induce hematological malignancies.

## Methods

### Ethics Statement

All experiments using the mice were performed in accordance with our institutional guidelines for the use of laboratory animals and approved by the review board for animal experiments of Chiba University (approval ID: 21–150).

### Generation of Mice

To generate tissue-specific *Bmi1*-transgenic mice, we used the plasmid *R26Stop$^{FL}$*, a modified version of pROSA26-1 with a *loxP*-flanked *neo$^r$*-stop cassette, an *frt*-flanked *IRES-eGFP* cassette, and a bovine polyadenylation sequence [34]. We cloned a cDNA encoding a flag-tagged *Bmi1* upstream of the *IRES* sequence (*R26Stop$^{FL}$Bmi1*). R1 ES cells were transfected, cultured, and selected as previously described [35]. For conditional expression of *Bmi1*, the *RosaStop$^{FL}$Bmi1* mice were crossed with *Tie2-Cre* mice. C57BL/6 (CD45.2) mice were purchased from Japan SLC (Shizuoka, Japan). C57BL/6 mice congenic for the Ly5 locus (CD45.1) were purchased from Sankyo-Lab Service (Tsukuba, Japan). Mice were bred and maintained in the Animal Research Facility of the Graduate School of Medicine, Chiba University in accordance with institutional guidelines. This study was approved by the institutional review committees of Chiba University (approval numbers 21–65 and 21–150).

### Flow Cytometric Analysis and Cell Sorting

Mouse $CD34^-LSK$ HSCs were purified from BM of 8–12-week-old mice. Mononuclear cells were isolated on Ficoll-Paque PLUS (GE Healthcare). Cells were stained with an antibody cocktail consisting of biotinylated anti-Gr-1, Mac-1, interleukin (IL)-7Rα, B220, CD4, CD8α, and Ter119 monoclonal antibodies. The monoclonal antibodies were purchased from eBioScience or BioLegend. Lineage-positive cells were depleted with goat anti-rat IgG microbeads (Miltenyi Biotec) through an LS column (Miltenyi Biotec). Cells were further stained with Alexa Fluor® 647 or eFluor® 660-conjugated anti-CD34, phycoerythrin (PE)-conjugated anti-Sca-1, and phycoerythrin/Cy7 (PE/Cy7)-conjugated anti-c-Kit antibodies. Biotinylated antibodies were detected with allophycocyanin/Cy7 (APC/Cy7)-conjugated streptavidin. Dead cells were eliminated by staining with Propidium iodide (1 μg/ml, Sigma). Analysis and sorting were performed on a FACS Aria II (BD Bioscience).

### Cell Cycle Analysis

Fresh BM cells ($1\times10^7$, CD45.2) were transplanted into 8-week-old CD45.1 mice irradiated at a dose of 9.5 Gy without competitor cells. Four months later, BM mononuclear cells were isolated on Ficoll-Paque PLUS. Cells were stained with an antibody cocktail consisting of biotinylated anti-Gr-1, Mac-1, IL-7Rα, B220, CD4, CD8α, Ter119, and CD45.1 monoclonal antibodies. Cells were further stained with Alexa Fluor® 700-conjugated anti-CD34, pacific blue-conjugated anti-Sca-1, and APC-conjugated anti-c-Kit antibodies. Biotinylated antibodies were detected with APC/Cy7-conjugated streptavidin. Analysis was performed on a FACS Aria II. To analyze the cell-cycle status, cells were incubated with 1 μg/ml Pyronin Y (Sigma) at 37°C for 45 min with protection from light. Bulk sorted $CD34^-LSK$ cells were incubated in SF-O3 supplemented with 50 μM?2-β-mercaptoethanol, 0.2% BSA, 1% GPS, 50 ng/ml SCF, 50 ng/ml TPO for 10 days at 37°C in a 5% $CO_2$ atmosphere. At day 10 of culture, the cell cycle profiles of culture cells were analyzed using an APC BrdU Flow Kit (BD Pharmingen). The cells were incubated with 10 μM BrdU at 37°C for 30 min and then stained with an antibody cocktail consisting of biotinylated anti-Gr-1,

Mac-1, IL-7Rα, B220, CD4, CD8α, and Ter119 monoclonal antibodies. Cells were further stained with PE-conjugated anti-Sca-1, and PE/Cy7-conjugated anti-c-Kit antibodies. Biotinylated antibodies were detected with APC/Cy7-conjugated streptavidin. Analysis was performed on a FACS Canto II (BD Bioscience).

## Colony Assay

Colony assays were performed in methylcellulose-containing Iscove's modified Dulbecco's medium (Methocult M3234; Stemcell Technologies) supplemented with 20 ng/ml mouse SCF, 20 ng/ml mouse IL-3, 20 ng/ml human TPO, and 3 U/ml human EPO (Peprotech), and incubated at 37°C in a 5% $CO_2$ atmosphere. The number of HPP- and LPP-colony-forming cells (CFCs), which generate a colony with a diameter ≥1 mm and <1 mm, respectively, were evaluated by counting colonies at day 10–14 of culture. Colonies were individually collected, cytospun onto glass slides, and subjected to Hemacolor (MERCK) staining for morphological examination. To evaluate the proliferative and differentiation capacity of *Tie2-Cre;R26Stop$^{FL}$Bmi1* HSCs *in vitro*, single CD34$^-$LSK HSCs were clonally sorted into 96-microtiter plates containing 100 µl SF-O3 (Sanko Junyaku) supplemented with 50 µM 2-β-mercaptoethanol, 10% FBS, 1% L-glutamine, penicillin, streptomycin solution (GPS; Sigma), 10 ng/ml mouse SCF, 10 ng/ml human TPO, 10 ng/ml mouse IL-3, and 3 unit/ml human EPO (PeproTech). At day 14 of culture, the colonies were counted and individually collected for morphological examination. To evaluate the tolerance of test cells against oxidative stress, CD34$^-$LSK cells were cultured in the presence of DL-Buthionin-(*S,R*)-sulfoximine (BSO, Sigma) or *N*-Acetyl-L-cysteine (NAC, Sigma) for the indicated time periods, then subjected to colony assays or flow cytometric analyses.

## Serial Transplantation and CRU Assays

Fresh BM cells ($5\times10^5$, CD45.2) or 10-day cultured CD34$^-$LSK cells (CD45.2) corresponding to 20 initial CD34$^-$LSK cells were transplanted into 8-week-old recipient mice (CD45.1) irradiated at a dose of 9.5 Gy together with $5\times10^5$ and $2\times10^5$ BM competitor cells from 8-week-old CD45.1 mice, respectively. For serial transplantation, BM cells were collected from all recipient mice at 12–20 weeks after transplantation and pooled together. Then, $5\times10^6$ BM cells were transplanted into 8-week-old B6-CD45.1 mice irradiated at a dose of 9.5 Gy without competitor cells. Third and fourth transplantation were similarly performed using $5\times10^6$ pooled BM cells. Peripheral blood (PB) cells of the recipient mice were analyzed with a mixture of antibodies that included PE/Cy7-conjugated anti-CD45.1, pacific blue-conjugated anti-CD45.2, PE-conjugated anti-Mac-1 and anti-Gr-1, APC-conjugated anti-B220, and APC/Cy7-conjugated anti-CD4 and anti-CD8α antibodies. Cells were analyzed on a FACS Canto II. Percent donor chimerism was calculated as (% donor cells) ×100/(% donor cells + % recipient cells). To obtain the competitive repopulating units (CRUs), CRU assays were performed with a limiting number of test cells and the data were analyzed using L-Calc software (StemCell Technologies). Peripheral blood cell counts were made using an automated cell counter, Celltec α (Nihon Kohden).

## Apoptosis Analysis

Bulk sorted CD34$^-$LSK cells were incubated in SF-O3 supplemented with 50 µM?2-β-mercaptoethanol, 0.2% BSA, 1% GPS, 50 ng/ml SCF, 50 ng/ml TPO for 10 days at 37°C in a 5% $CO_2$ atmosphere. At day 10 of culture, the cultured cells were incubated with APC-conjugated anti-Annexin V (BD Pharmingen) and propidium iodide at room temperature for 15 min with protection from light. Analysis was performed on FACS Canto II.

## Immunostaining of γH2A.X

Cells were incubated in a culture medium drop on slide glasses pre-treated with poly-L-lysine (Sigma) for 2 hours. After fixation with 2% paraformaldehyde and blocking in 4% sheep serum for 30 min at room temperature, cells were incubated with purified anti-phospho-Histone H2A.X (Ser139) antibody (Cell Signaling Technology) for 12 hours at 4°C. The cells were then washed and incubated with Alexa Flour 555-conjugated anti-rabbit IgG goat polyclonal antibody (Invitrogen) for 60 min at room temperature. DNA was counterstained with 4′,6-diamidino-2-phenylindole (DAPI). Images were taken with a Keyence BZ-9000 fluorescence microscope.

## RT-PCR

Total RNA was isolated using TRIZOL LS solution or TRIZOL solution (Invitrogen) and reverse transcribed by the ThermoScript RT-PCR system (Invitrogen) with an oligo-dT primer. Real-time quantitative polymerase chain reaction (PCR) was performed with an ABI prism 7300 Thermal Cycler (Applied Biosystems) using FastStart Universal Probe Master (Roche). The combination of primer sequences and probe numbers are as follows: for *p16$^{Ink4a}$*, probe #91, 5′-AATCTCCGCGAGGAAGC-3′, and 5′-GTCTGTCTGCAGCGGACTC-3′; for *p19$^{Arf}$*, probe #106, 5′-GGGTTTTCTTGGTGAAGTTCG-3′, 5′- TTGCCCATCATCATCACCT-3′, and for *Bmi1*, probe #95, 5′-AAACCAGACCACTCCTGAACA-3′ and 5′-TCTTCTTCTCTTCATCTCATTTTTGA-3′.

## Western Blotting

Total cell lysate was resolved by SDS-PAGE and transferred to a PVDF membrane. The blots were probed with a mouse anti-Bmi1 (clone 8A9, kindly provided by Dr. N. Nozaki, MAB Institute, Co. Ltd., Japan), and a horseradish peroxidase-conjugated secondary antibody. The protein bands were detected with an enhanced chemiluminescence reagent (SuperSignal, Pierce Biotechnology).

## Detection of ROS

Cells were stained with an antibody cocktail consisting of biotinylated anti-Gr-1, Mac-1, IL-7Rα, B220, CD4, CD8α, and Ter119 monoclonal antibodies. Cells were further stained with PE-conjugated anti-Sca-1, and PE/Cy7-conjugated anti-c-Kit antibodies. Biotinylated antibodies were detected with APC/Cy7-conjugated streptavidin. After staining with antibodies, cells were incubated with CellROX$^{TM}$ Deep Red Reagent (5 µM, Invitrogen) at 37°C for 30 min with protection from light. Dead cells were eliminated by staining with propidium iodide (1 µg/ml, Sigma). Analysis was performed on a FACS Aria II.

# Supporting Information

**Figure S1 Steady state hematopoiesis in *Tie2-Cre;R26-StopFLBmi1* mice.** (A) Hematopoietic analysis of 10-week-old *Tie2-Cre* and *Tie2-Cre;R26Stop$^{FL}$Bmi1* mice. Absolute numbers of CMPs, GMPs, MEPs, and CLPs in bilateral femurs and tibiae (upper panels), total spleen cells and LSK cells in the spleen (middle panel), and total thymic cells, CD4+CD8- cells, CD4-CD8+ cells, and CD4+CD8+ cells in the thymus (lower panels) are shown as the mean ± S.D. (*Tie2-Cre*; n = 8, *Tie2-Cre;R26-Stop$^{FL}$Bmi1*; n = 7). (B) Cell cycle status of CD34-LSK cells examined by Pyronin Y incorporation. Proportion of CD34-

LSK cells in the G0 phase of the cell cycle (Pyronin Y-) was shown as the mean ± S.D. (n = 4) (left panel). Representative flow cytometric profiles are also depicted (right panel).
(EPS)

**Figure S2 Apoptosis and cell cycle status of *Tie2-Cre;R26Stop$^{FL}$Bmi1* LSK cells in culture.** (A) The proportion of apoptotic cells in the LSK fraction in culture. CD34-LSK cells from *Tie2-Cre* (Control) and *Tie2-Cre;R26Stop$^{FL}$Bmi1* (Bmi1) mice were cultured in the SF-O3 serum-free medium supplemented with 50 ng/ml SCF and TPO. At day 10 of culture, apoptotic cells were detected by staining culture cells with anti-Annexin V and propidium iodide (PI). The percentage of Annexin V+PI- apoptotic cells in the LSK fraction is shown as the mean ± S.D. (n = 5). (B) The cell cycle status of LSK cells overexpressing Bmi1. CD34-LSK cells from *Tie2-Cre* (Control) and *Tie2-Cre;R26-Stop$^{FL}$Bmi1* (Bmi1) mice were cultured in the SF-O3 serum-free medium supplemented with 50 ng/ml SCF and TPO. At day 10 of culture, the cells were incubated with 10 μM BrdU at 37°C for 30 min and then analyzed using a BrdU Flow Kit. Data are shown as the mean ± SD (n = 4).
(EPS)

**Figure S3 Hematopoietic recovery in recipients of *Tie2-Cre;R26Stop$^{FL}$Bmi1* HSCs after irradiation.** Fresh BM cells from *Tie2-Cre* and *Tie2-Cre;R26Stop$^{FL}$Bmi1* mice (1×107, CD45.2) were transplanted into 8-week-old CD45.1 mice irradiated at a dose of 9.5 Gy without competitor cells. Four months later, the recipient mice were irradiated at a dose of 5 Gy. Changes in the PB cell count were monitored for 4 weeks (A) and the absolute number of BM LSK cells in bilateral femurs and tibiae was examined at 4 weeks post-irradiation (B). Data are shown as the mean ± SD (n = 5).
(EPS)

**Figure S4 ROS levels in *Tie2-Cre;R26Stop$^{FL}$Bmi1* cells in culture.** Levels of ROS in cells overexpressing Bmi1 in culture. CD34-LSK cells from *Tie2-Cre* (Control) and *Tie2-Cre;R26-Stop$^{FL}$Bmi1* (Bmi1) mice were cultured in the SF-O3 serum-free medium supplemented with 50 ng/ml SCF and TPO. Cells from day 11 or 12 of culture were further cultured for 2 days in the presence of 0.2 mM BSO, then levels of ROS in Lin-Sca-1+c-Kit+ cells and Lin-Sca-1low/−c-Kit+ cells were analyzed using CellROXTM Deep Red Reagent. Data are shown as dots and the mean values are indicated by bars (n = 4).
(EPS)

## Acknowledgments

We thank Naohito Nozaki for the anti-Bmi1 antibody, George Wendt for critical reading of the manuscript, and Mieko Tanemura for laboratory assistance.

## Author Contributions

Conceived and designed the experiments: SN AI. Performed the experiments: SN M. Oshima JY AS SM TK SY M. Osawa. Analyzed the data: SN AI. Contributed reagents/materials/analysis tools: HK HN. Wrote the paper: SN AI.

## References

1. Simon JA, Kingston RE (2009) Mechanisms of polycomb gene silencing: knowns and unknowns. Nat Rev Mol Cell Biol 10: 697–708.
2. Iwama A, Oguro H, Negishi M, Kato Y, Nakauchi H (2005) Epigenetic regulation of hematopoietic stem cell self-renewal by polycomb group genes. Int J Hematol 81: 294–300.
3. Konuma T, Oguro H, Iwama A (2010) Role of the polycomb group proteins in hematopoietic stem cells. Dev Growth Differ 52: 505–516.
4. Sauvageau M, Sauvageau G (2010) Polycomb group proteins: multi-faceted regulators of somatic stem cells and cancer. Cell Stem Cell 7: 299–313.
5. Lessard J, Sauvageau G (2003) Bmi-1 determines the proliferative capacity of normal and leukaemic stem cells. Nature 423: 255–260.
6. Park IK, Qian D, Kiel M, Becker MW, Pihalja M, et al. (2003) Bmi-1 is required for maintenance of adult self-renewing haematopoietic stem cells. Nature 423: 302–305.
7. Iwama A, Oguro H, Negishi M, Kato Y, Morita Y, et al. (2004) Enhanced self-renewal of hematopoietic stem cells mediated by the polycomb gene product Bmi-1. Immunity 21: 843–851.
8. Oguro H, Iwama A, Morita Y, Kamijo T, van Lohuizen M, et al. (2006) Differential impact of Ink4a and Arf on hematopoietic stem cells and their bone marrow microenvironment in Bmi1-deficient mice. J Exp Med 203: 2247–2253.
9. Oguro H, Yuan J, Ichikawa H, Ikawa T, Yamazaki S, et al. (2010) Poised lineage specification in multipotent hematopoietic stem and progenitor cells by the polycomb protein Bmi1. Cell Stem Cell 6: 279–286.
10. Mihara K, Chowdhury M, Nakaju N, Hidani S, Ihara A, et al. (2006) Bmi-1 is useful as a novel molecular marker for predicting progression of myelodysplastic syndrome and patient prognosis. Blood 107: 305–308.
11. Rizo A, Horton SJ, Olthof S, Dontje B, Ausema A, et al. (2010) BMI1 collaborates with BCR-ABL in leukemic transformation of human CD34+ cells. Blood 116: 4621–4630.
12. Kisanuki YY, Hammer RE, Miyazaki J, Williams SC, Richardson JA, et al. (2001) Tie2-Cre transgenic mice: a new model for endothelial cell-lineage analysis in vivo. Dev Biol 230: 230–242.
13. Takano H, Ema H, Sudo K, Nakauchi H (2004) Asymmetric division and lineage commitment at the level of hematopoietic stem cells: inference from differentiation in daughter cell and granddaughter cell pairs. J Exp Med 199: 295–302.
14. Ema H, Takano H, Sudo K, Nakauchi H (2000) In vitro self-renewal division of hematopoietic stem cells. J Exp Med 192: 1281–1288.
15. Shima H, Takubo K, Iwasaki H, Yoshihara H, Gomei Y, et al. (2009) Reconstitution activity of hypoxic cultured human cord blood CD34-positive cells in NOG mice. Biochem Biophys Res Commun 378: 467–472.
16. Ito K, Hirao A, Arai F, Takubo K, Matsuoka S, et al. (2006) Reactive oxygen species act through p38 MAPK to limit the lifespan of hematopoietic stem cells. Nat Med 12: 446–451.
17. Yahata T, Takanashi T, Muguruma Y, Ibrahim AA, Matsuzawa H, et al. (2011) Accumulation of oxidative DNA damage restricts the self-renewal capacity of human hematopoietic stem cells. Blood 118: 2941–2950.
18. Rossi DJ, Jamieson CH, Weissman IL (2008) Stems cells and the pathways to aging and cancer. Cell 132: 681–696.
19. Chagraoui J, Hébert J, Girard S, Sauvageau G (2011) An anticlastogenic function for the Polycomb Group gene Bmi1. Proc Natl Acad Sci USA 108: 5284–5289.
20. Ginjala V, Nacerddine K, Kulkarni A, Oza J, Hill SJ, et al. (2011) BMI1 is recruited to DNA breaks and contributes to DNA damage-induced H2A ubiquitination and repair. Mol Cell Biol 31: 1972–1982.
21. Facchino S, Abdouh M, Chatoo W, Bernier G (2010) BMI1 confers radioresistance to normal and cancerous neural stem cells through recruitment of the DNA damage response machinery. J Neurosci 30: 10096–10111.
22. Shao L, Li H, Pazhanisamy SK, Meng A, Wang Y, et al. (2010) Reactive oxygen species and hematopoietic stem cell senescence. Int J Hematol 94: 24–32.
23. Jang YY, Sharkis SJ (2007) A low level of reactive oxygen species selects for primitive hematopoietic stem cells that may reside in the low-oxygenic niche. Blood 110: 3056–3063.
24. Liu J, Liu C, Chen J, Song S, Lee IH, et al. (2009) Bmi1 regulates mitochondrial function and the DNA damage response pathway. Nature 459: 387–392.
25. Rizo A, Olthof S, Han L, Vellenga E, de Haan G, et al. (2009) Repression of BMI1 in normal and leukemic human CD34$^+$ cells impairs self-renewal and induces apoptosis. Blood 114: 1498–1505.
26. Owusu-Ansah E, Banerjee U (2009) Reactive oxygen species prime Drosophila haematopoietic progenitors for differentiation. Nature 461: 537–541.
27. Bracken AP, Kleine-Kohlbrecher D, Dietrich N, Pasini D, Gargiulo G, et al. (2007) The polycomb group proteins bind throughout the INK4A-ARF locus and are disassociated in senescent cells. Genes Dev 21: 525–530.
28. Negishi M, Saraya A, Mochizuki S, Helin K, Koseki H, et al. (2010) A novel zinc finger protein Zfp277 mediates transcriptional repression of the Ink4a/Arf locus through polycomb repressive complex 1. PLoS One 5: e12373.
29. Kamminga LM, Bystrykh LV, de Boer A, Houwer S, Douma J, et al. (2006) The Polycomb group gene Ezh2 prevents hematopoietic stem cell exhaustion. Blood 107: 2170–2179.
30. Stapels M, Piper C, Yang T, Li M, Stowell C, et al. (2010) Polycomb group proteins as epigenetic mediators of neuroprotection in ischemic tolerance. Sci Signal 3: ra15.
31. Bracken AP, Helin K (2009) Polycomb group proteins: navigators of lineage pathways led astray in cancer. Nat Rev Cancer 9: 773–784.

32. Diehn M, Cho RW, Lobo NA, Kalisky T, Dorie MJ, et al. (2009) Association of reactive oxygen species levels and radioresistance in cancer stem cells. Nature 458: 780–783.
33. Zhou J, Bi C, Cheong LL, Mahara S, Liu SC, et al. (2011) The histone methyltransferase inhibitor, DZNep, up-regulates TXNIP, increases ROS production, and targets leukemia cells in AML. Blood 118: 2830–2839.
34. Sasaki Y, Derudder E, Hobeika E, Pelanda R, Reth M, et al. (2006) Canonical NF-kappaB activity, dispensable for B cell development, replaces BAFF-receptor signals and promotes B cell proliferation upon activation. Immunity 24: 729–739.
35. Fukamachi H, Fukuda K, Suzuki M, Furumoto T, Ichinose M, et al. (2001) Mesenchymal transcription factor Fkh6 is essential for the development and differentiation of parietal cells. Biochem Biophys Res Commun 280: 1069–1076.

# MT1-MMP plays a critical role in hematopoiesis by regulating HIF-mediated chemokine/cytokine gene transcription within niche cells

Chiemi Nishida,[1] Kaori Kusubata,[2] Yoshihiko Tashiro,[1] Ismael Gritli,[1] Aki Sato,[1] Makiko Ohki-Koizumi,[1] Yohei Morita,[1] Makoto Nagano,[3] Takeharu Sakamoto,[3] Naohiko Koshikawa,[3] Takahiro Kuchimaru,[4] Shinae Kizaka-Kondoh,[4] Motoharu Seiki,[3] Hiromitsu Nakauchi,[1] *Beate Heissig,[1,2,5] and *Koichi Hattori[1,5]

[1]Center for Stem Cell Biology and Regenerative Medicine, Institute of Medical Science, University of Tokyo, Tokyo, Japan; [2]Frontier Research Initiative, Institute of Medical Science, University of Tokyo, Tokyo, Japan; [3]Division of Cancer Cell Research, Institute of Medical Science, University of Tokyo, Tokyo, Japan; [4]Department of Biomolecular Engineering, Tokyo Institute of Technology, Yokohama, Japan; and [5]Atopy (Allergy) Research Center, Juntendo University School of Medicine, Tokyo, Japan

**HSC fate decisions are regulated by cell-intrinsic and cell-extrinsic cues. The latter cues are derived from the BM niche. Membrane-type 1 matrix metalloproteinase (MT1-MMP), which is best known for its proteolytic role in pericellular matrix remodeling, is highly expressed in HSCs and stromal/niche cells. We found that, in MT1-MMP$^{-/-}$ mice, in addition to a stem cell defect, the transcription and release of kit ligand (KitL), stromal cell–derived factor-1 (SDF-1/CXCL12), erythropoietin (Epo), and IL-7 was impaired, resulting in a trilineage hematopoietic differentiation block, while addition of exogenous KitL and SDF-1 restored hematopoiesis. Further mechanistic studies revealed that MT1-MMP activates the hypoxia-inducible factor-1 (HIF-1) pathway via factor inhibiting HIF-1 (FIH-1) within niche cells, thereby inducing the transcription of HIF-responsive genes, which induce terminal hematopoietic differentiation. Thus, MT1-MMP in niche cells regulates postnatal hematopoiesis, by modulating hematopoietic HIF-dependent niche factors that are critical for terminal differentiation and migration. (*Blood*. 2012;119(23):5405-5416)**

## Introduction

The adult hematopoietic system is maintained by a small number of HSCs that reside in the BM in a specialized microenvironment (the niche).[1,2] Here, HSCs undertake fate decisions including differentiation to progenitor cells and self-renewal, which ensures a lifelong supply of terminally differentiated blood cells. Intrinsic cellular programming and external stimuli such as adhesive interactions with the microenvironmental stroma and cytokine activities regulate HSC fate. However, it is unclear how niche factor production is controlled to adjust to external demand with a fine-tuned response.

Hypoxia-inducible factors (HIFs) consist of an α (HIF-α) and a β (HIF-β, or ARNT) subunit and activate the expression of genes encoding proteins that regulate cell metabolism, motility, angiogenesis, hematopoiesis, and other functions. HSCs maintain cell-cycle quiescence by regulating HIF-1α levels.[3,4] Mice with mutations in the heterodimeric transcription factor HIF develop extensive hematopoietic pathologies: embryos lacking *Arnt* have defects in primitive hematopoiesis.[5] Mice lacking endothelial PAS domain protein 1 (EPAS1, also known as HIF-2alpha/HRF/HLF/MOP3), a second HIF family member, exhibited pancytopenia, and it was shown that EPAS1 is necessary to maintain a functional microenvironment in the BM for effective hematopoiesis.[6] HIFs bind to canonical DNA sequences in the promoters or enhancers of target genes such as erythropoietin (*Epo*), vascular endothelial growth factor-A, *SDF-1*α/CXCL12, angiopoietin-2, platelet-derived growth factor-B and Kit Ligand (*KitL*)/stem cell factor, which are involved in HSC maintenance within the BM niche.[7-10] The chemokine SDF-1α/CXCL12 (SDF-1α) is expressed by perivascular, endosteal, mesenchymal stem and progenitor cells as well as by osteoblasts.[11,12] SDF-1α deficiency leads to a reduction in HSCs and impaired B-cell development in mice.[13,14] IL-7 is another stromal cell–derived niche factor, which, in cooperation with CXCL12, functions at sequential stages of B-cell development.[15,16] IL-7 or IL-7R deficiency results in impaired B-cell development.[17,18]

Proteases such as matrix metalloproteinase-9 (MMP-9) and the serine proteinase plasmin(ogen) regulate HSC fate through KitL release in the BM.[10,19] Membrane type-1 MMP (MT1-MMP, also known as MMP-14) can proteolytically degrade extracellular matrix (ECM) components and cleave membrane receptors and ligands.[20] MT1-MMP is expressed within mesenchymal stem and immature hematopoietic cells.[21,22] MT1-MMP can control the migration of hematopoietic stem/progenitor cells and monocytes.[21,23,24] MT1-MMP function is essential for angiogenesis, wound healing, connective tissue remodeling, arthritis, tumor growth, and metastasis.[25-27] MT1-MMP–deficient (MT1-MMP$^{-/-}$) mice showed skeletal dysplasia, arthritis, and osteopenia.[28] However, the role of MT1-MMP in hematopoiesis is unclear.

We found that MT1-MMP inactivation in mice resulted in severe pancytopenia, characterized by an impaired stem cell pool and a block in hematopoietic differentiation. MT1-MMP deletion from hematopoietic cells generated normal hematopoiesis in recipient mice, thereby demonstrating that MT1-MMP is an essential regulator of the BM microenvironment. Mechanistically, we demonstrate that MT1-MMP deficiency blocked the transcription of

Submitted November 8, 2011; accepted April 21, 2012. Prepublished online as *Blood* First Edition paper, April 27, 2012; DOI 10.1182/blood-2011-11-390849.

*B.H. and K.H. share senior authorship.

The online version of this article contains a data supplement.

The publication costs of this article were defrayed in part by page charge payment. Therefore, and solely to indicate this fact, this article is hereby marked "advertisement" in accordance with 18 USC section 1734.

typical HIF-1–dependent niche factors including Epo, SDF-1, KitL, and IL-7 by modulating the HIF-1 pathway through factor inhibiting HIF-1 (FIH1), resulting in a 3-lineage terminal differentiation block. Thus, MT1-MMP controls HSC fate by regulating the BM niche.

## Methods

### Animals

Age-matched (14-day) MT1-MMP$^{+/+}$ and MT1-MMP$^{-/-}$ mice were obtained by heterozygous breeding.[24] Animal procedures were approved by the Animal Care Committee of The Institute of Medical Science (University of Tokyo). C57BL/6 and C57BL/6-Tg (CAG-EGFP) mice were purchased from Japan SLC Inc, and Ly5.1 mice were purchased from Sankyo Lab Service.

### In vivo assays

***Competitive transplantation experiments.*** Lethally irradiated Ly-5.1 mice were injected with BM cells (10 recipient mice per cell concentration) from MT1-MMP$^{+/+}$ or MT1-MMP$^{-/-}$ mice together with $2 \times 10^5$ CD45.1 BM competitive cells. Peripheral blood (PB) cells of the recipient mice were analyzed 4 months after transplantation. Cells were stained with PE-conjugated anti-CD4 and anti-CD8, FITC-conjugated anti-CD45.2, allophycocyanin-conjugated anti-CD11b and anti-Gr-1, PE-cy7–conjugated anti-B220, and biotinylated anti-CD45.1 Abs. The biotinylated Ab was developed using streptavidin-PE–Cy5. The percentage of donor-derived lineage contributions in PBMCs was assessed using Abs against CD45.2, Gr-1/CD11b, or B220. Total chimerism of $> 1\%$ for all Abs tested using PBMCs was considered as long-term reconstitution. The frequencies were determined using L-Calc software (StemCell Technologies).

***Growth factor rescue experiments.*** Recombinant mouse KitL (PeproTech) was administered IP into MT1-MMP$^{+/+}$ and MT1-MMP$^{-/-}$ mice at a concentration of 150 μg/kg body weight, daily from postnatal day 7 to day 10. Recombinant mouse SDF-1α (PeproTech; 100 ng/mice) was injected twice intraperitoneally on postnatal day 10. Blood was collected and blood cells counted on day 12.

***CFU-S assay.*** Mobilized PBMCs were obtained and subjected to a CFU-S assay as previously described.[29] Mice were killed on day 12. The number of visible splenic colonies was counted.

### In vitro assays

***Peripheral blood analysis.*** Blood was collected from mice by retro-orbital bleeding using heparinized capillaries. White blood cell (WBC), RBC, and platelet (PLT) counts were determined. Plasma samples were stored at −80°C until further analysis.

***Hematopoietic progenitor assay.*** BM mononuclear cells (BMMCs; $10^4$ cells/plate) were plated in triplicate in 1 mL of a commercially available methylcellulose-based assay solution (Methocult; StemCell Technologies).

***Lineage-negative cell separation.*** Murine BM cells were obtained after flushing mouse femur and tibiae. Cells were stained using a lineage cell separation kit (StemCell Technologies). After MACS cell separation (Miltenyi Biotec), cells were stained with c-Kit, Sca-1, and lineage Abs (BD Pharmingen), and were then analyzed by FACS.

***B-cell colony-forming assay (CFU–IL-7).*** The CFU–IL-7 assay was carried out in medium (Invitrogen) containing 1.2% methylcellulose (StemCell Technologies), 30% FCS (HyClone), 1% BSA, 0.1mM 2-ME, and mouse IL-7 (PeproTech). On day 7 of culture, aggregates consisting of $> 50$ cells were scored as a colony.

***Cell culture.*** Mouse stromal cells (MS-5) were maintained in IMDM supplemented with 10% FBS. Human BM endothelial cells (BMEC-1) were maintained in Medium 199 supplemented with 10% FBS, 0.146 mg/mL L-glutamine, and 2.2 mg/mL sodium bicarbonate. Mouse embryonic fibroblast cells (NIH3T3) were maintained in DMEM supplemented with 10% FBS. These cells were cultured at 37°C, in a 5% $CO_2$ incubator. Human osteoblastic cells (FOB) were maintained in a 1:1 mixture of Ham F12 medium DMEM supplemented with 2.5mM L-glutamine and 10% FBS, and the cells were cultured at 34°C, in a 5% $CO_2$ incubator. MT1-MMP$^{+/+}$ and MT1-MMP$^{-/-}$ mouse embryonic fibroblasts (MEF) cells (kindly provided by M.S.) were maintained in DMEM (Invitrogen) supplemented with 10% FBS at 37°C, in a 5% $CO_2$ incubator.[30]

***Knockdown experiment using shRNA.*** The shRNA sequences used for knockdown of mouse MT1-MMP and FIH-1 were: 5′-caccgctgtggtgttc-cggataagtcgaaacttatccggaacaccacagc-3′ and 5′-caccggacctcgaatacctgcaagac-gaatcttgcaggtattcgaggtcctttt-3′, respectively. These sequences were subcloned into pENTR/U6 TOPO (Invitrogen) and then transferred via recombination into the lentivirus vector pLenti6 BLOCKiT (Invitrogen). shRNA-expressing lentiviral vectors were generated and used according to the manufacturer's instructions.

***FACS analysis.*** Cells were flushed out from mouse BM. For cell-surface analysis, cells were stained with the following Abs: PE-conjugated anti-CD19, -Sca-1, -B220, CD44, c-kit, and -Gr1, FITC-conjugated anti-CD43, -CD34, -NK1.1, and -CD8, allophycocyanin-conjugated anti-B220, -CD4, CD11b, and a lineage cocktail, PerCP-Cy5.1–conjugated anti-c-kit. Cells were analyzed using FACS Aria (BD Biosciences). Common myeloid progenitor (CMP), granulocyte/macrophage progenitor (GMP), and megakaryocyte/erythroid progenitor (MEP) were determined in Lin$^-$ BM cells of 14-day-old MT1-MMP$^{+/+}$ and MT1-MMP$^{-/-}$ mice. The following Abs were used: c-kit–allophycocyanin, Sca1-PE/Cy7, CD34-FITC, FcgRIII-PE all from BD Pharmingen. For the detection of Lin$^-$ cells, biotinylated Abs (B220-bio, Gr-1-bio, CD11b-bio, CD5-bio, Ter119-bio, 7-4-bio, from Miltenyi Biotec) were costained with allophycocyanin/Cy7-conjugated (BD Biosciences/BD Pharmingen) streptavidin. For mesenchymal stem cells (MSCs) detection, cells were stained with the following Abs: CD45-PE, Sca1-FITC, PDGFRα-allophycocyanin (eBioscience), TER119-PE (BD Bioscience), CD45–Pacific Blue (BioLegend), and Alexa 488–conjugated nestin Ab (Abcam).

***RNA extraction, RT-PCR, and quantitative real-time PCR analysis.*** Total RNA was extracted using RNA TRIzol (Invitrogen), and cDNA was generated according to the manufacturer's protocols. This cDNA (10 ng) was used as a template for each PCR amplification using the following specific forward and reverse primers, respectively: mouse *β-actin* (5′-tggaatcctgtggcatccatgaaac-3′) and (5′-taaaacgcagctcagtaacagtccg-3′); mouse *MT1-MMP* (5′-tccggataagtttgggactg-3′) and (5′-ccttcaccatcaaagggtgt-3′); human *GAPDH* (5′-gagtcaacggatttggtcgt-3′) and (5′-ttgattttggagggatctcg-3′); human *MT1-MMP* (5′-caagcattgggtgtttgatgatg-3′) and (5′-cttggggtactcgctatcca-3′). For quantitative real-time PCR, PCR mixtures were prepared using SYBR Premix Ex TaqII (Takara) containing 0.2mM of each primer, and amplification reactions were performed. Specific forward and reverse primers, respectively, were designed as follows: *β-actin* (5′-gctggaaggtggacagtgag-3′) and (5′-tgacaggatgcagaaggaga-3′); *KitL* (5′-gcctagtcattgttggctac-3′) and (5′-cccaagtttgtctatgatgg-3′); *SDF-1* (5′-agaaaccttccaccagagca-3′) and (5′-aacggctaggaaagggtctc-3′); *IL-7* (5′-tgcaatcatgtcaactgcaa-3′) and (5′-tgcaatcatgtcaactgcaa-3′); *EPO* (5′-catctgcgacagtcgagttctg-3′) and (5′-cacaacccatcgtgacattttc-3′); *G-CSF* (5′-cctgcttagagcagagagag-3′) and (5′-cagcagcaggaatcaatact-3′). Gene expression levels were measured using the ABI Prism 7500 sequence detection system (Applied Biosystems). PCR product levels were estimated by measurement of the intensity of SYBR Green fluorescence. Gene expression levels were normalized to *β-actin* mRNA.

***Knockdown experiment using siRNA.*** Target sequences for siRNA were commercially designed and synthesized (B-bridge). siRNAs were provided as a mixture containing 3 different siRNA target sequences. The RNAi transfection solution was prepared by preincubating a mixture of 5nM siRNAs dissolved in 1 mL of serum-free and antibiotic-free medium (OptiMEM; Invitrogen) and 10 μL of RNAiMAX for 20 minutes at room temperature. Cells ($3\text{-}4.5 \times 10^5$ cell/4 mL growth medium without antibiotics) suspended by trypsinization were added to the mixture and cultured overnight, and the medium was replaced with fresh growth medium.

***Overexpression of MT1-MMP.*** The transfection solution was prepared by preincubating a mixture of 1 μg of plasmid DNA dissolved in 250 μL of OptiMEM and 3 μL of Lipofectamine 2000 (Invitrogen) dissolved in 250 μL of OptiMEM for 20 minutes at room temperature. The transfection mixture (500 μL in total) was then added to the cells. After

48 hours of culture, the culture media were replaced with fresh growth medium.

***Immunoprecipitation.*** Cells were lysed with cell lysis buffer (Cell Signaling Technology) and the supernatants were collected. Total protein content was measured using the Bradford assay (Bio-Rad). Lysates were incubated with protein-G–Sepharose beads (Santa Cruz Biotechnology) and anti–HIF-1α Ab (BD Biosciences) overnight and were then spun down for 1 minute at 5800*g*. The supernatant was removed and the pellets were solubilized with 6 × SDS sample buffer (0.35M Tris-HCl, pH 6.8, 10% SDS, 30% glycerol, 9.3% DTT) and analyzed by immunoblot analysis.

***Immunoblotting.*** Cells were lysed with lysis buffer (Cell Signaling Technology) according to the manufacturer's instructions. The supernatants were collected, and total protein content was measured using the Bradford assay (Bio-Rad). The subcellular proteome extraction kit (Merck) was used to fractionate subcellular proteins. Lysates were separated by SDS-PAGE, transferred to a PVDF membrane, subjected to immunoblotting using anti–FIH-1 (1:200; Santa Cruz Biotechnology), anti-integrinβ1 (1/1000; Chemicon), and anti-α/β tubulin (1:1000; Cell Signaling Technology), washed with TBS-T, and immunoprobed for 1 hour at room temperature with HRP-conjugated or alkaline phosphatase–conjugated Ab, then washed with PBS-T. Finally, membranes were incubated with ECL-Plus (Amersham), and the chemiluminescent signal was detected using LAS4000 (Fujifilm) according to the manufacturer's instructions. The alkaline phosphatase signal was then detected using the Histofine Kit (Nichirei).

***Immunoassay.*** After cell transfection with siRNA, the growth medium was replaced and the cells were cultured for 48 hours. Supernatants were then collected and analyzed for murine KitL, SDF-1α, and IL-7 using commercially available ELISAs (R&D Systems).

***Stromal-based expansion cultures.*** A total of $1 \times 10^4$ $Lin^-$ cells from the BM of GFP mice were cocultured with a confluent layer of stromal cells (MS-5). Recombinant mouse KitL (20 ng/mL, every other day) or recombinant mouse SDF-1α (100 ng/mL, every other day) was added to MT1-MMP KD MS-5 and control MS-5 cell cultures. Twelve days later, adherent cells were retrieved using trypsin (Sigma-Aldrich) and pooled with the nonadherent cells. Hematopoietic cells (GFP positive) were counted.

***Migration assay.*** Migration assays were performed in 24-well plates using 5-μm polycarbonate Transwell inserts (Costar). BM $Lin^-$ cells were collected and isolated from normal adult mice. The cells were resuspended in X-vivo 15 (Lonza). MT1-$MMP^{+/+}$ and MT1-$MMP^{-/-}$ MEF culture supernatant was aliquoted (600-μL aliquots) into 24-well plates, which formed the bottom chamber, in the presence or absence of neutralizing Abs against mouse SDF-1 (R&D Systems). $Lin^-$ cells derived from the BM cells of GFP mice ($2 \times 10^5$ cells in 100 μL) were added into the Transwell insert (top chamber), and the cells were allowed to migrate through the porous bottom for 4 hours at 37°C. The number of cells that migrated into the lower chamber was determined using flow cytometry. Cells had been stained with Abs against CD11b and Gr1 (BD Biosciences). The medium from the lower chamber was passed through a FACSCalibur for 60 seconds, gating on forward (FSC) and side scatter to exclude cell debris. The number of live cells was compared with a 100% migration control in which $2 \times 10^5$ cells had been added directly into the lower chamber and then counted on the FACScalibur for 60 seconds.

***Immunohistochemistry.*** BM sections were fixed with 4% paraformaldehyde and permeabilized using 0.2% Triton X-100 for 20 minutes. After blocking in PBS containing 5% goat serum and 0.2% BSA, the sections were incubated with anti–FIH-1 Ab (Novus Biologicals) for 16 hours, washed 3 times with PBS and incubated for 1 hour with anti–rabbit Alexa 568 (Invitrogen). After washing, the sections were incubated with Alexa 488–conjugated nestin Ab (Abcam) for 2 hours. For HIF-1 staining, fixed and blocked sections were incubated with Alexa 488–conjugated HIF-1 Ab (BD Pharmingen) for 2 hours. The sections were mounted using Vectashield Mounting Medium with DAPI (Vector Laboratories). Images were acquired with an Olympus DP71 camera.

***Micro-CT analysis.*** We evaluated the BM shaft surface area by using micro-CT (Rigaku). We measured the shaft area at the center of the femur by NIH ImageJ software.

***Proliferation assay.*** A total of $2 \times 10^4$ $Lin^-$ cells isolated by MACS (Miltenyi Biotec) from BM cells of GFP mice were cocultured with a confluent layer of MEF cells. The cells were maintained in X-vivo 15 supplemented recombinant mouse IL-3 (20 ng/mL, every other day) with or without neutralizing Abs against mouse KitL (R&D Systems). One week later, all cells were retrieved using trypsin (Sigma-Aldrich). GFP-positive were counted using FACS.

### Statistical analysis

Data were analyzed using the unpaired 2-tailed Student *t* test and are expressed as means ± SEM. *P* values of $< .05$ were considered significant.

## Results

### MT1-MMP deletion leads to severe pancytopenia

We used 14-day-old MT1-$MMP^{-/-}$ mice to explore the role of MT1-MMP in the regulation of postnatal hematopoiesis, as mortality of older MT1-$MMP^{-/-}$ mice is very high.[24,28] Compared with MT1-$MMP^{+/+}$ mice, the body weight of MT1-$MMP^{-/-}$ mice was decreased (7.22 ± 0.48 and 2.99 ± 0.05 g/mouse, respectively; n = 5, $P < .001$) and there was a decline in all hematopoietic lineages examined in MT1-$MMP^{-/-}$ animals, including WBCs (Figure 1A), PLTs (Figure 1B), and RBCs (Figure 1C) in the PB. MT1-$MMP^{-/-}$ hematopoietic femurs were smaller than MT1-$MMP^{+/+}$ femurs (Figure 1D). Under steady-state conditions, BM cellularity in MT1-MMP mice was decreased compared with MT1-$MMP^{+/+}$ mice (Figure 1E). We next analyzed the number of MSCs by flow cytometry. The frequency of $PDGFR\alpha^+/Sca1^+/CD45^-/Ter119^-$ BM-derived MSCs and $nestin^+$ niche cells was lower in MT1-$MMP^{-/-}$ BM cells than in MT1-$MMP^{+/+}$ BM cells (Figure 1F).[31] Because the skeletal malformation described in MT1-$MMP^{-/-}$ mice could affect the intrafemural space where hematopoiesis occurs, the BM shaft surface area was determined by microcomputer tomography (microCT). The BM shaft surface area was reduced in MT1-$MMP^{-/-}$ femurs compared with MT1-$MMP^{+/+}$ mice (Figure 1G).

Histologic analysis of BM sections showed that MT1-$MMP^{-/-}$ mice exhibited a striking paucity of hematopoietic cells within the BM shaft and a reduction in the number of megakaryocytes, which are responsible for platelet production (Figure 1H-I).

We next examined HSCs and hematopoietic progenitor populations. In wild-type mice, MT1-MMP is expressed in primary BMMCs within the lineage-negative ($Lin^-$) cell fraction, which contains mostly hematopoietic progenitor cells and a small fraction of HSCs, and in BM stromal cells, including BM endothelial cells (BMEC-1), fetal osteoblasts (FOB), and fibroblast-like stromal cells (MS-5; Figure 1J-K). The absolute number of CFU cells (CFU-C; Figure 1L) and of more primitive progenitor populations within BM cells, including day-8 CFU-spleen (CFU-S; Figure 1M), CMPs, GMPs, and MEPs and HSC-enriched $CD34^-c\text{-}Kit^+$, $Sca\text{-}1^+$, $Lin^-$ (KSL) cells were diminished in MT1-$MMP^{-/-}$ BMMCs. To determine the HSC content of the BM, we performed limiting-dilution competitive repopulation analysis using MT1-$MMP^{+/+}$ or MT1-$MMP^{-/-}$ BMMCs. There was a lower frequency, and a significantly reduced absolute number of competitive repopulation units (CRUs) per femur in MT1-$MMP^{-/-}$ BMMCs than in MT1-$MMP^{+/+}$ BMMCs. These data indicate that MT1-MMP is required for HSC maintenance and for normal hematopoietic differentiation.

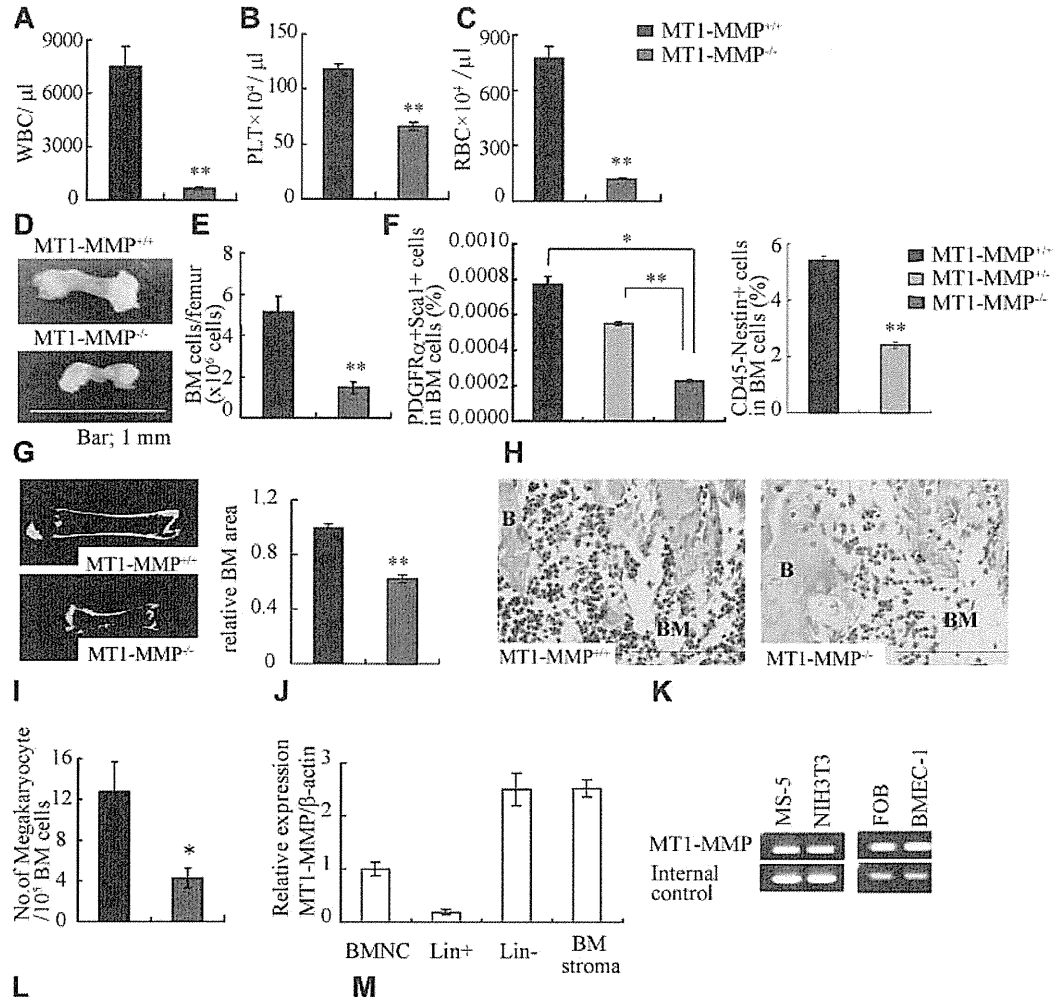


M

| | MT1-MMP$^{+/+}$ | MT1-MMP$^{-/-}$ | p value |
|---|---|---|---|
| Frequency in BM cells | | | |
| CMP (%) | 0.8 ± 0.12 | 1.1 ± 0.16 | 0.40 |
| GMP (%) | 2.4 ± 0.16 | 2.7 ± 0.038 | 0.19 |
| MEP (%) | 6.0 ± 0.52 | 7.7 ± 0.31 | 0.04 |
| CFU-S (%) | 0.009 ± 0.002 | 0.016 ± 0.003 | 0.06 |
| CD34-KSL (%) | 0.02 ± 0.003 | 0.01 ± 0.001 | 0.44 |
| CRU | 1/38269 | 1/76281 | 0.08 |
| Absolute number in BM cells (cells / femur) | | | |
| CMP | 61136 ± 8543 | 28095 ±2522 | <0.001 |
| GMP | 166418 ± 23153 | 75271 ± 7910 | <0.001 |
| MEP | 423860 ± 56766 | 212591 ± 17432 | < 0.005 |
| CFU-S | 3127 ± 93 | 994 ± 78 | < 0.005 |
| CD34-KSL | 1166 ± 16 | 248 ± 24 | <0.001 |
| CRU | 128 ± 12 | 24 ± 2 | <0.001 |

**Figure 1. MT1-MMP gene deletion causes myelosuppression.** (A-C) The number of (A) WBCs, (B) platelets (PLT), and (C) RBCs in the PB of 14-day-old mice was counted (n = 8). (D) Images of mouse femurs (bars, 1 mm). (E) Total BM cell number per femur. (F) The percentage of PDGFRα$^+$Sca1$^+$ cells (MSCs) was determined by flow cytometry (n = 2). (G) (left panel) Representative MicroCT scan images, and (right panel) quantification of the relative BM area within the BM femur shaft are presented (n = 3). (H) H&E-stained femur sections. Right panel shows the quantification of the BM area per femur. B indicates bone, (bars, 200 μm). (I) Megakaryocyte number (n = 5). (J-K) Real-time PCR analysis of MT1-MMP expression in (J) BM nuclear cells (BMNCs), Lin$^+$, Lin$^-$, and BM stroma cells, and (K) in MS-5, NIH3T3, FOB, and BMEC-1 cells. (L-M) The (L) absolute number of CFU-C per $10^5$ BM cells and (M) frequency and absolute number/femur of CFU-S, CMP, GMP, MEP, CD34-KSL cells, and competitive repopulating units (CRU) in wild-type and knockout BM cells (n = 3). For CRU determination, freshly isolated BM cells of different cell concentration were transplanted into recipients (n = 10). Four months posttransplantation, the repopulating unit (RU) with trilineage engraftment (> 1% of donor-derived cells) was calculated. The absolute number of CRU was calculated based on the observed number of BM cells per femur. Errors in bar graphs are SEM; *$P < .05$, **$P < .01$. CFU-C indicates CFU cells; CFU-S, CFU-spleen; CMP, common myeloid progenitor; GMP, granulocyte/macrophage lineage-restricted progenitor; and MEP, megakaryocyte/erythrocyte lineage-restricted progenitor.

### MT1-MMP$^{-/-}$ mice show a T- and B-cell differentiation defect

Compared with MT1-MMP$^{+/+}$ mice, the absolute numbers of PB CD3$^+$ T and B220$^+$ B lymphocytes were reduced (Figure 2A) and the spleen was much smaller (Figure 2B) in MT1-MMP$^{-/-}$ mice. Similar to the BM, histologic examination revealed less megakaryocytes in the MT1-MMP$^{-/-}$ spleen (Figure 2C). The white pulp appeared smaller in MT1-MMP$^{-/-}$ spleens (Figure 2C), which correlated with a reduction in the absolute numbers of lymphoid

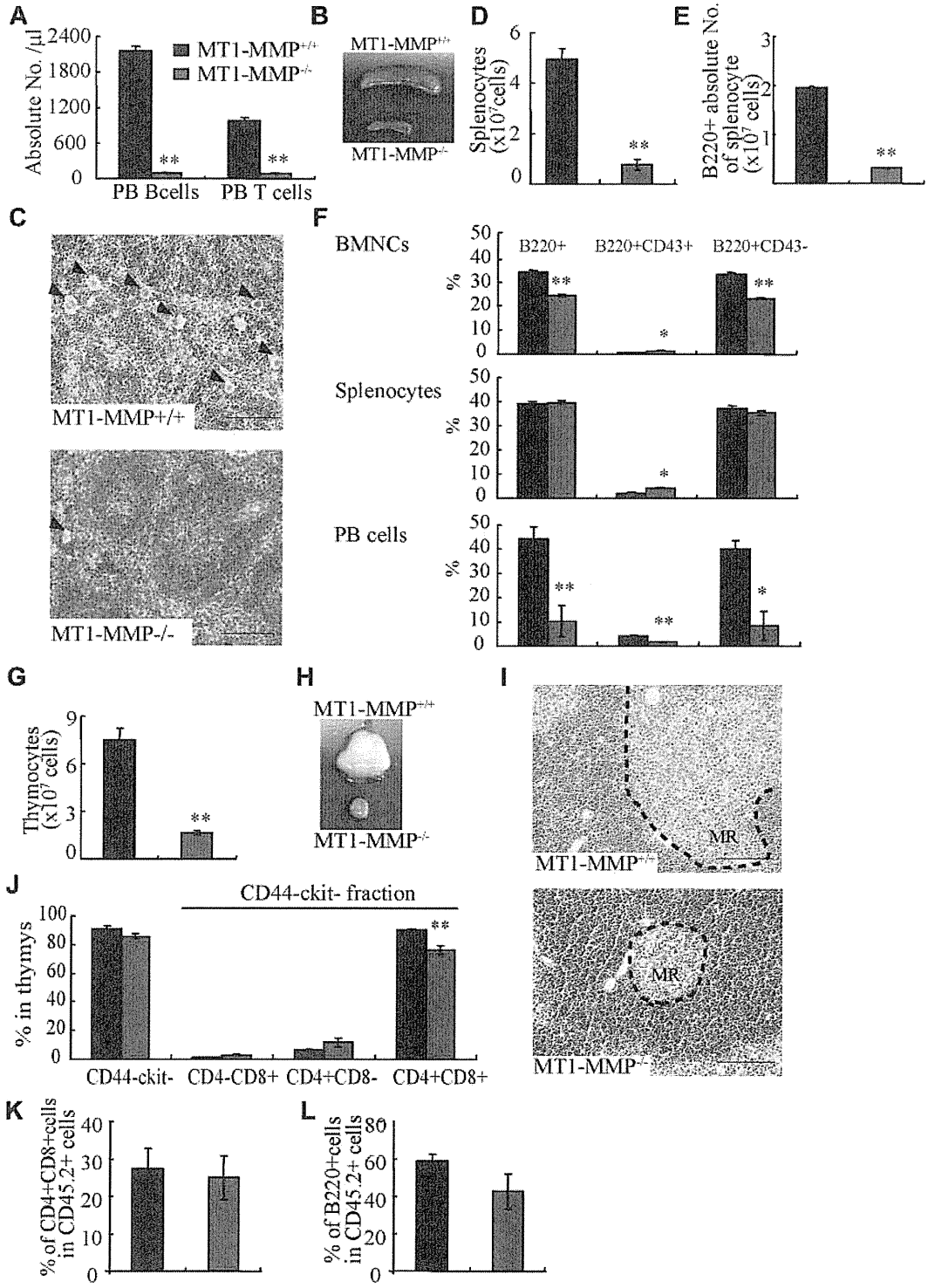


**Figure 2. T and B lymphopoiesis are impaired in MT1-MMP$^{-/-}$ mice.** (A) PB B- and T-cell numbers (FACS analysis). (B) Images of mouse spleens. (C) H&E-stained spleen sections. Arrowheads indicate megakaryocytes (bars, 100 μm). (D-E) The (D) total number of splenocytes and (E) B220$^+$ cells in splenocytes (n ≥ 6). (F) The percentage of B220$^+$ populations in BMNCs (n = 6), splenocytes (n = 3), and PB cells (n = 2). (G) Thymocyte number (n = 4). (H) Images of thymi. (I) H&E-stained thymus sections. MR indicates medullar region (bars, 100 μm). (J) The percentage of thymic T-lineage subpopulations. (K-L) BM cells from MT1-MMP$^{+/+}$ and MT1-MMP$^{-/-}$ mice were transplanted into wild-type animals (CD45.2). (K) The percentage of donor CD4$^+$/CD8$^+$ T and (L) B220$^+$B cell lineage contribution of donor-derived cells in the PB 4 months after transplantation (n = 10/group). Errors in bar graphs are SEM; *$P < .05$, **$P < .01$.

and total B (B220$^+$) spleen cells (Figure 2D-E). The percentage of B220$^+$, early- (B220$^+$CD43$^+$), and late-stage (B220$^+$CD43$^-$) B cells was reduced in MT1-MMP$^{-/-}$ BM, spleen, and PBMCs (Figure 2F). Although the absolute number of early- and late-stage B cells in splenocytes was reduced in MT1-MMP$^{-/-}$ mice (data not shown), the relative percentage of early (B220$^+$CD43$^+$) B cells was augmented in MT1-MMP$^{-/-}$ splenocytes. These data demonstrate that MT1-MMP is required for normal terminal B-cell differentiation within the BM with impaired release of B cells into the circulation.

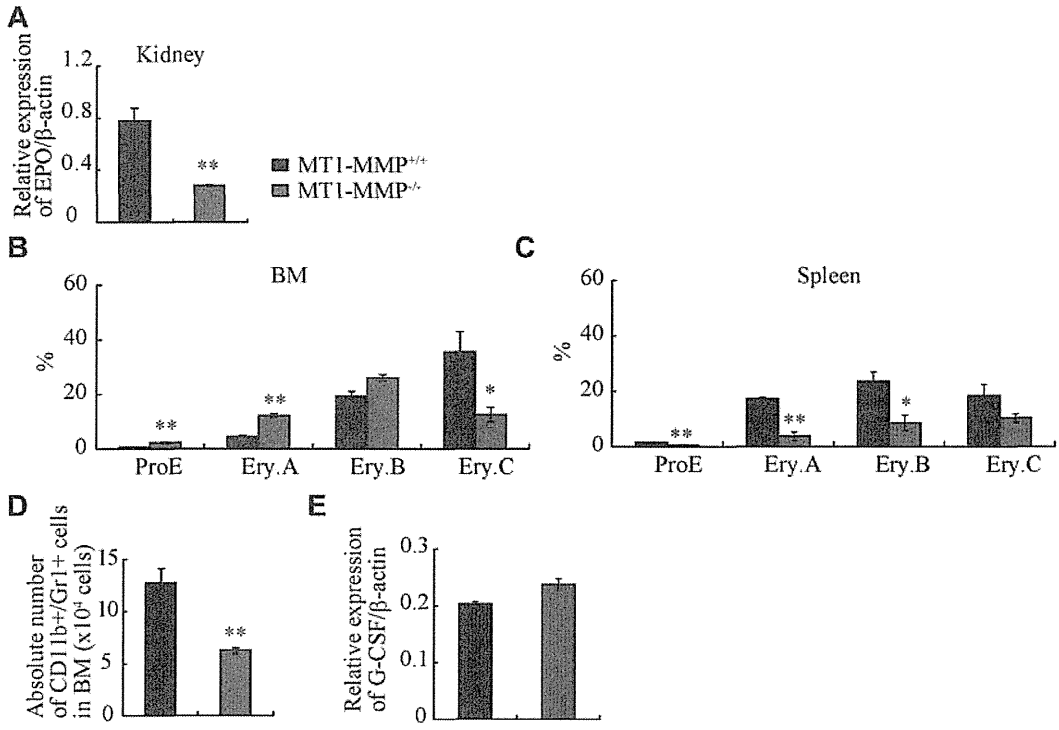


**Figure 3. Erythroid and myeloid differentiation block in MT1-MMP$^{-/-}$ mice.** (A) Real-time PCR of *Epo* in kidney (n = 3). (B-C) Percentage of different erythroblast populations during erythroid development (proE-EryA-EryB-EryC) of (B) BM cells or of (C) dissociated mouse spleen cells from MT1-MMP$^{+/+}$ (n = 5) and MT1-MMP$^{-/-}$ mice (n = 3). (D) Percentage of CD11b$^{+}$/Gr-1$^{+}$ cells per femur as determined by FACS (n = 5). Errors in bar graphs are SEM; $^{**}P < .01$. (E) Real-time PCR of *G-CSF* in BM cells (n = 3).

The earliest T-cell progenitors are produced in the BM. We found an increase in the percentage of immature CD4$^{-}$CD8$^{-}$c-Kit$^{-}$CD44$^{-}$ cells T cells in MT1-MMP$^{-/-}$ BM cells ($4.1 \times 10^5 \pm 0.2 \times 10^5$ cells in MT1-MMP$^{-/-}$ and $2.6 \times 10^5 \pm 0.3 \times 10^5$ cells in MT1-MMP$^{+/+}$ BM, respectively; n = 4, $P < .05$). The MT1-MMP$^{-/-}$ thymus (Figure 2G) was small with a low number of thymocytes (Figure 2H). Thymic lobes, and specifically the medullar region, appeared smaller than in MT1-MMP$^{+/+}$ mice (Figure 2I). Flow cytometric analysis of thymocytes revealed no difference in the percentage of immature CD4$^{-}$ or CD8$^{-}$ double-negative (DN) thymocytes or of CD4$^{-}$CD8$^{-}$c-Kit$^{-}$CD44$^{-}$ thymocytes between the MT1-MMP$^{+/+}$ and the MT1-MMP$^{-/-}$ mice. However, a relative decrease in the percentage of the more mature CD4$^{+}$CD8$^{+}$ double-positive (DP) thymocyte population and in the CD4$^{+}$ single-positive (SP) cell population was revealed in thymocytes from the MT1-MMP$^{-/-}$ mice (Figure 2J). In absolute terms, CD4 SP numbers were reduced 2.5-fold, CD8 SP 2.1-fold, and DP thymocytes 5.3-fold, whereas the DN population remained unaffected. These data indicate that T-cell progenitors developed within the BM even in the absence of MT1-MMP, but that their further differentiation in the thymus was blocked at or before development of the immature DN thymocyte population, causing default differentiation into CD4 cell SP and NK-cell lineages.

To assess whether the abnormal thymic colonization observed in MT1-MMP$^{-/-}$ mice was because of the loss of MT1-MMP in hematopoietic cells or in stromal cells, MT1-MMP$^{+/+}$ and MT1-MMP$^{-/-}$ BM donor cells were transplanted into lethally irradiated wild-type recipients. Chimeras were analyzed 4 months after transplantation. T- and B-cell differentiation of transplanted MT1-MMP$^{-/-}$ cells (expressing the Ag Ly5.2 (CD45.2) on leukocytes) within the BM were normal (Figure 2K-L). These data indicated that MT1-MMP$^{-/-}$ mice showed impaired T- and B-cell development. Even though MT1-MMP$^{-/-}$ mice showed a hematopoietic cell defect (see Figure 1), MT1-MMP$^{-/-}$ BM cells retained the potential to differentiate into T- and B-cell lineages in an MT1-MMP$^{+/+}$ environment. These data indicate that, aside from its influence on stem cells, MT1-MMP also plays an additional role in regulating the BM niche.

### MT1-MMP ablation impairs erythroid and myeloid differentiation

Anemia, as seen in 14-day-old MT1-MMP mice (see Figure 1C), is expected to trigger a compensatory response that is mediated principally through increased serum levels of erythropoietin (*Epo*), a master cytokine of erythropoiesis. Epo controls growth, survival, and differentiation of erythroid progenitors, either cooperatively with, or independently of KitL.[32-34] Despite severe anemia, *Epo* mRNA expression in kidney tissues of MT1-MMP$^{-/-}$ mice was low (Figure 3A) and the expected compensatory increase in spleen size did not occur (see Figure 2B).

To assess erythroid differentiation, we examined CD71 and TER119 expression in the BM and splenic erythroblasts, and classified erythroid cells into 4 populations at progressive levels of differentiation: proerythroblasts TER119$^{med}$CD71$^{high}$FSC$^{high}$ (ProE), TER119$^{high}$CD71$^{high}$FSC$^{high}$ (Ery.A), TER119$^{high}$CD71$^{high}$FSC$^{low}$ (Ery.B), and TER119$^{high}$CD71$^{low}$FSC$^{low}$ (Ery.C).[35]

MT1-MMP$^{-/-}$ BM erythroid lineage cells accumulated at the ProE, Ery.A, and Ery.B stage, and cells at the late erythroblast differentiation stages (Ery.C) were reduced (Figure 3B). In spleen, all stages of erythroid lineage cells were reduced in MT1-MMP$^{-/-}$ mice (Figure 3C). These data suggest that MT1-MMP is involved in both BM and splenic erythropoiesis, and that the defect in erythropoiesis in MT1-MMP$^{-/-}$ mice might be due, in part, to impaired Epo production.

Granulocytic cells of adult mouse BM express CD11b and high amounts of Gr-1. The absolute number of $CD11b^+/Gr\text{-}1^+$ granulocytes was lower in MT1-$MMP^{-/-}$ than in MT1-$MMP^{+/+}$ BM cells (Figure 3D). G-CSF is a growth, differentiation, and activating factor for neutrophils and their precursors. Regardless of the observed neutropenia, no difference in *G-CSF* (Figure 3E) or thrombopoietin (*Tpo*; data not shown) expression was observed in the BM cells of these mice, indicating that other factors might be responsible for the impaired myelopoiesis.

### MT1-MMP deficiency reduces stromal cell–derived cytokine production

Chimera experiments indicated that the observed hematopoietic defect in MT1-MMP–deficient mice was in part because of a niche defect, suggesting that dysregulated production of stromal cell–derived cytokine(s) may be responsible for the hematopoietic differentiation block observed in MT1-$MMP^{-/-}$ mice. BM and thymic stromal cells produce IL-7.[36] Plasma levels of the stromal cell–derived factors KitL, SDF-1α, and IL-7 were lower in MT1-$MMP^{-/-}$ mice than in MT1-$MMP^{+/+}$ mice (Figure 4A-C). We observed a reduced number of $nestin^+$ niche cells in MT1-$MMP^{-/-}$ mice and, interestingly, $nestin^+$ niche cells highly express KitL and SDF-1.[31] In accordance with these data, MT1-$MMP^{-/-}$ BM cells and MT1-$MMP^{-/-}$ primary stromal cells showed lower mRNA expression of *IL-7, KitL*, and *SDF-1α/CXCL12* compared with MT1-$MMP^{+/+}$ cells (Figure 4D, supplemental Figure 1). In addition, very few primary stromal cells grew in cultures established using MT1-$MMP^{-/-}$ BM cells (supplemental Figure 1).

To exclude the possibility that the growth/chemokine factor decrease in MT1-$MMP^{-/-}$ mice was because of a lower number of the growth factor–producing stromal cells, we modulated MT1-MMP expression on a murine stromal cell line (MS-5). Overexpression of MT1-MMP in MS-5 stromal cells (MT1-MMP TF) increased *KitL, SDF-1α*, and *IL-7* gene expression (Figure 4E). In contrast, MT1-MMP knock down in MS-5 murine stromal cells using shRNA (*MT1-MMP KD*) reduced the expression of *KitL, SDF-1α*, and *IL-7* mRNA than control MS-5 cells (Figure 4F). Consistent with this result, less KitL, SDF-1α, and IL-7 protein was detected in supernatants of MT1-MMP KD cultures compared with control cultures as determined by ELISA (Figure 4G). The frequency of CXCR4 (the SDF-1 receptor) and c-Kit (the KitL receptor) expressing $Sca\text{-}1^+$ MT1-$MMP^{-/-}$ BMMCs was not significantly changed (data not shown). These data indicate that loss of MT1-MMP activity in stromal cells reduced signaling by IL-7, KitL, and SDF-1α, factors known to regulate B and T lymphopoiesis and erythropoiesis.

We next examined the release and expression of these factors by primary *MEFs*. Confirming our BM cell and primary stromal cell cytokine/chemokine data, low expression of *KitL, SDF-1α*, and *IL-7* was found in MT1-$MMP^{-/-}$ MEFs (Figure 4H-I).

To investigate whether the observed impaired production of cytokines/chemokines would also result in impaired function, we set up an MEF feeder–based culture supplemented with IL-3. Whereas $Lin^-$ cells differentiated in MT1-$MMP^{+/+}$ MEF-supported cultures, the number of $CD11b^+/Gr\text{-}1^+$ cells in MT1-$MMP^{-/-}$ cultures did not change significantly (Figure 4J). Addition of neutralizing Abs against KitL confirmed that the observed myeloid cell differentiation was mainly because of the KitL that was released by the cultures.

We set up a migration assay to investigate SDF-1α function. $Lin^-$ cells derived from BM cells migrated toward an MT1-$MMP^{+/+}$ MEF supernatant, a process that is mediated by SDF-1, as shown by using neutralizing Abs against SDF-1. In contrast, no migration of $Lin^-$ cells was observed toward an MT1-$MMP^{-/-}$ supernatant (Figure 4K).

### MT1-MMP increases cytokine/chemokine production in niche cells by suppressing HIF-1α

The *HIF* gene is known to regulate VEGF, placental growth factor, angiopoietin 2, platelet-derived growth factor-B, SDF-1α, Epo, and KitL/SCF expression.[7] HIF-1α activity under normoxia depends on the FIH-1. FIH1-mediated hydroxylation disrupts a critical interaction between HIFα and the coactivators p300/CBP, impairing HIF transcriptional activity.[37,38] To determine whether HIF signaling is involved in MT1-MMP modulation of hematopoietic differentiation, we assessed HIF-1α, HIF-2α, and FIH-1 protein levels in MT1-MMP knockdown and control MS-5 cells. MT1-MMP knockdown did not affect HIF-1α or HIF-2α protein expression (supplemental Figure 2), but did up-regulate FIH-1 protein expression within the cytosol of MS-5 cells (Figure 5A), where FIH-1 can prevent HIF-1α binding to the transcriptional coactivator p300/CBP thereby blocking HIF-1-induced transcription of genes such as SDF-1 and KitL.[39] Immunohistochemical analysis showed that less $nestin^+$ stromal cells coexpressing FIH-1 were found in MT1-$MMP^{-/-}$ BM cells than in MT1-$MMP^{+/+}$ BM cells (Figure 5B). These findings are consistent with previous data that, in monocytes, the cytoplasmic tail of MT1-MMP binds to FIH-1, leading to inhibition of FIH-1 activity by its inhibitor, Mint3/APBA3.[23]

HIF-1 immunostaining showed that HIF-1, in contrast to its expression in MT1-$MMP^{+/+}$ BM cells, was preferentially expressed in the cytoplasm of MT1-$MMP^{-/-}$ BM cells (Figure 5C).

Our data suggested that MT1-MMP can activate the HIF1 pathway in stromal cells as it does in monocytes. We therefore hypothesized that FIH-1 overexpression in stromal cells would cause a reduction in cytokine/chemokine production, which was indeed the case (Figure 5D-F). These data suggested that FIH-1 overexpression reduced SDF-1, KitL, and IL-7 gene transcription in stromal cells. Furthermore, although the knockdown efficiency of FIH-1 by shRNA was only 30%, FIH-1 knockdown rescued *KitL, SDF-1α*, and *IL-7* gene expression in MT1-MMP knockdown (70% reduction by siRNA) MS-5 cells (Figure 5G-I) indicating that the decreased HIF-mediated cytokine gene transcription in MT1-MMP knockdown stromal cells can be partially rescued by blocking FIH-1 activity. These data highlight the importance of MT1-MMP–mediated HIF-1 activation for the transcriptional regulation of critical hematopoietic niche factors.

### Exogenous SDF-1α and KitL addition restores leukopenia and thrombopenia in MT1-$MMP^{-/-}$ mice

Finally, we asked whether growth factor addition would rescue the observed block in leukopenia and thrombopenia because of MT1-MMP deficiency. Indeed, addition of recombinant IL-7 to MT1-$MMP^{-/-}$ or wild-type BMMC cultures induced a similar number of B-cell colonies (CFU–IL-7) in the MT1-$MMP^{-/-}$ as in the wild-type cells (Figure 6A).

MS-5 cells support myeloid cell differentiation of $Lin^-$ wild-type cells in vitro. However, fewer $GFP^+$ hematopoietic cells were generated from $Lin^-$ wild-type BM cells on MT1-MMP KD MS-5 stromal cells than on control MS-5 cells. Addition of KitL restored hematopoietic cell growth on the MT1-MMP KD MS-5 feeder cultures (Figure 6B).

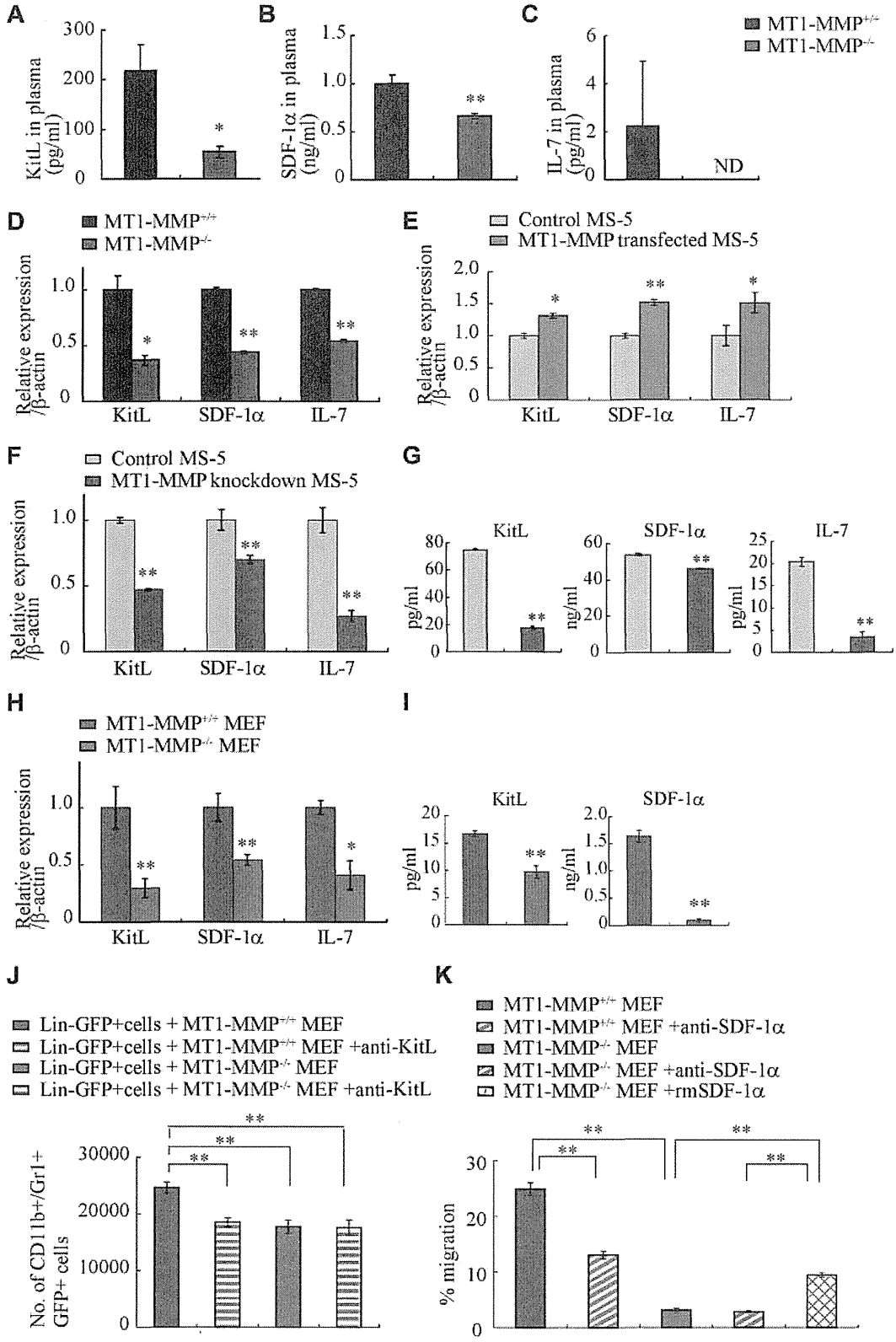


**Figure 4. MT1-MMP deficiency prevents transcription of niche chemokines/cytokines.** (A-C) KitL, SDF-1α, and IL-7 plasma levels in MT1-MMP$^{+/+}$ and MT1-MMP$^{-/-}$ plasma were measured by ELISA (n > 6). *KitL*, *SDF-1α*, and *IL-7* gene expression in (D) total BM cells, (E) MS-5 control and MT1-MMP–overexpressing cells, and (F) MT1-MMP knockdown (KD) and control MS-5 cells were analyzed using real-time PCR. The results are expressed relative to expression of a *β-actin*. (G) KitL, SDF-1α, and IL-7 protein levels in MT1-MMP knockdown (KD) and control MS-5 cell-culture supernatants were determined by ELISA. (H) *KitL*, *SDF-1α*, and *IL-7* gene expression in MT1-MMP$^{+/+}$ and MT1-MMP$^{-/-}$ MEF cells was determined using real-time PCR. The results are expressed relative to expression of *β-actin*. (I) KitL and SDF-1α protein levels in the indicated MEF cell-culture supernatants were evaluated by ELISA. (J) Lin$^{-}$GFP$^{+}$ cells were cultured on MT1-MMP$^{+/+}$ and MT1-MMP$^{-/-}$ MEF cells in the presence or absence of neutralizing Abs against KitL. The number of CD11b$^{+}$Gr1$^{+}$ cells was assessed after 7 days by FACS (n = 5). (K) Lin$^{-}$ cells were plated in transwells. MT1-MMP$^{+/+}$ and MT1-MMP$^{-/-}$ MEF cell-culture supernatants supplemented with recombinant SDF-1α were added to the lower chamber. Neutralizing Abs against SDF-1α were added to both chambers. The percentage of migrated cells was determined (n = 9 from 2 independent experiments). Errors in bar graphs are SEM; $^{*}P < .05$, $^{**}P < .01$. Data shown are representative of 3 to 4 independent experiments.

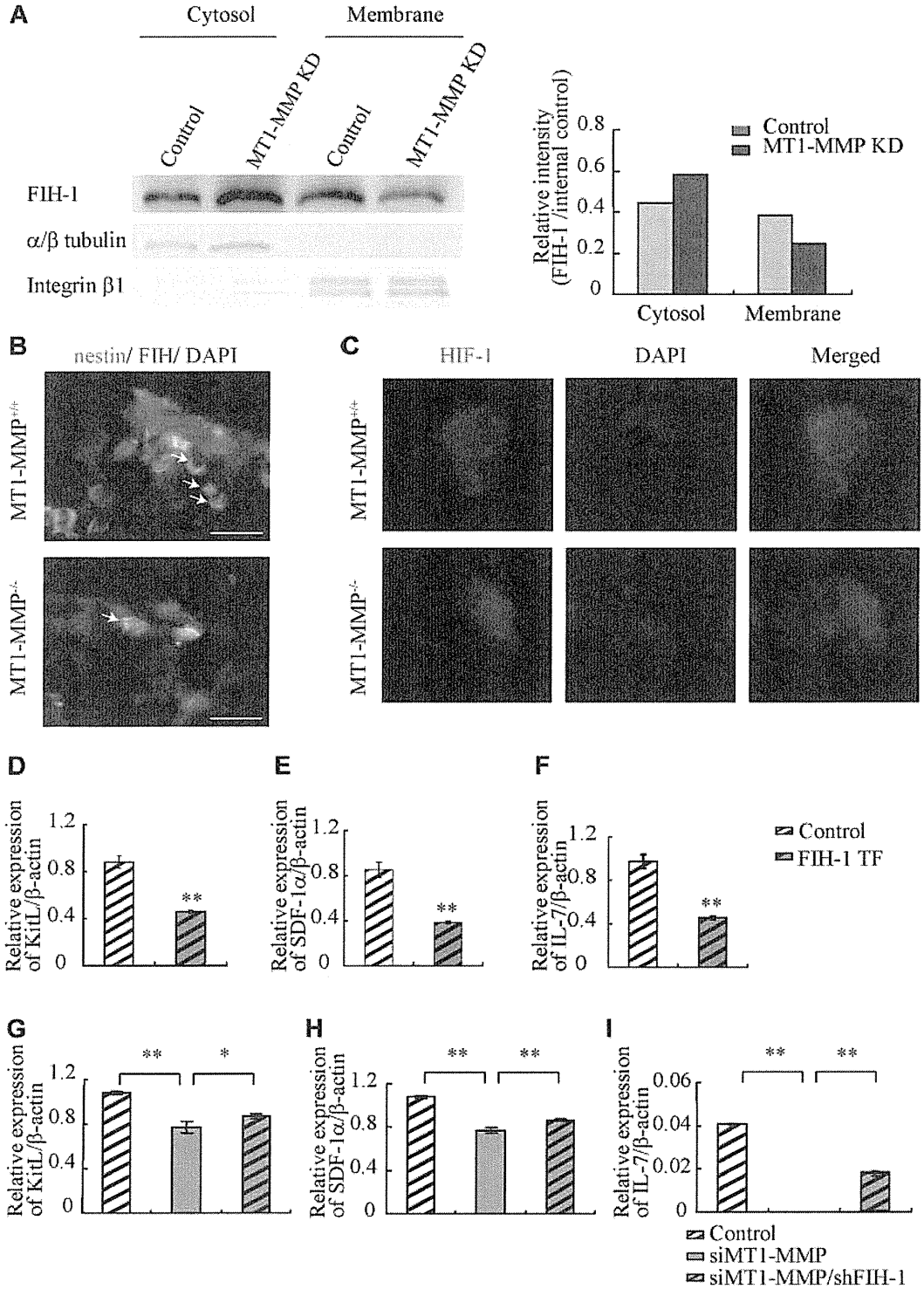


**Figure 5. MT1-MMP deficiency prevents HIF-mediated transcription of niche factors.** (A) FIH-1 expression in subcellular fractions was analyzed by Western blotting. α/β tubulin and integrin-β1 are representative cytosolic and membrane proteins, respectively. (B) Representative images of immunofluorescent staining of nestin (green fluorescence) and FIH-1 (red fluorescence) in BM sections derived from MT1-MMP$^{+/+}$ and MT1-MMP$^{-/-}$ mice. The arrows indicate nestin$^{+}$/FIH-1 cells. Nuclei were counterstained with DAPI (blue; bars, 100 μm). (C) Representative images of immunofluorescent staining of HIF-1α (green fluorescence) in BM cells derived from MT1-MMP$^{+/+}$ and MT1-MMP$^{-/-}$ mice. Nuclei were counterstained with DAPI (blue). (D-I) *KitL*, *SDF-1α* and *IL-7* gene expression in (D-F) MS-5 cells overexpressing FIH-1, and (G-I) in MT1-MMP–deficient MS-5 cells with or without *FIH-1* knockdown as analyzed using real-time PCR. The results are expressed relative to expression of a *β-actin*, which was set at 1.0. Data shown are representative of 3 to 4 independent experiments.

Similarly, KitL treatment restored WBC and PLT numbers in the PB in MT1-MMP$^{-/-}$ mice to the values of wild-type controls (Figure 6C-D) and a single injection of SDF-1α increased both WBC and PLT counts in the PB of MT1-MMP$^{-/-}$ mice 2 days after injection (Figure 6E-F). Although hematopoietic cell growth was restored in MT1-MMP$^{-/-}$ mice by injection of KitL or SDF-1, survival was not improved (data not shown).

Collectively, these results suggest that MT1-MMP alters the HSC niche by modulating HIF signaling, which promotes cytokine production and enhances cell differentiation and migration.

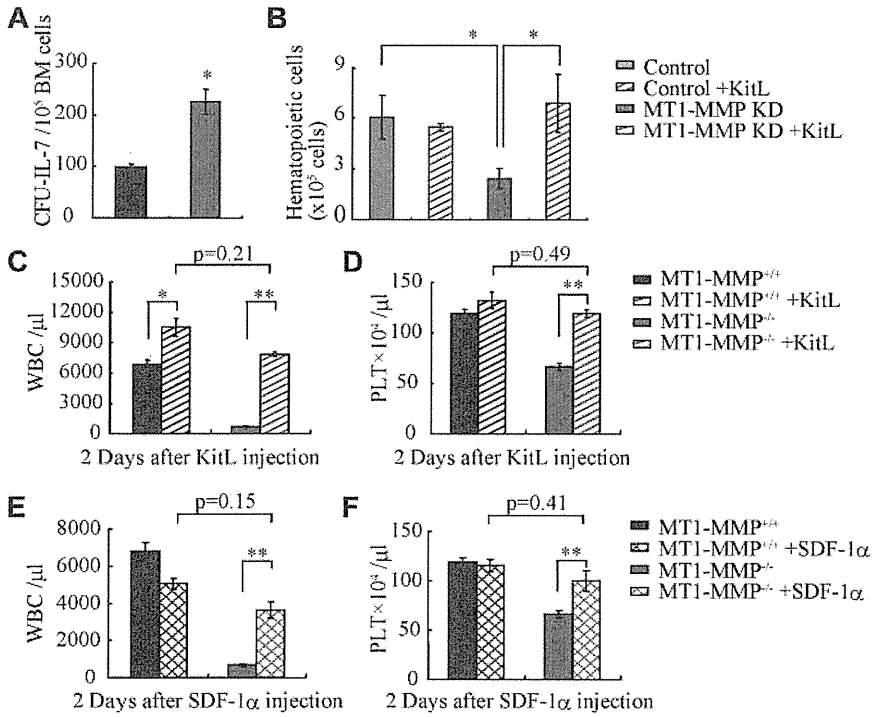


**Figure 6. MT1-MMP–deficient mice have a defective BM stromal niche with impaired terminal differentiation because of impaired release of HIF-1α–associated factors.** (A) Number of colonies in IL-7–containing cultures of MT1-MMP$^{+/+}$ and MT1-MMP$^{-/-}$ BM cells (n = 3). (B) Coculture of wild-type Lin$^-$ BM GFP$^+$ cells on confluent MT1-MMP knockdown or control MS-5 cells with/without KitL. (C-D) PB WBCs (C) and PLT (D) after KitL injections into MT1-MMP$^{+/+}$ (n ≥ 10) and MT1-MMP$^{-/-}$ mice (n = 3). (E-F) PB WBCs (E) and PLT (F) counts 2 days after initiation of SDF-1 treatment of MT1-MMP$^{+/+}$ (n ≥ 10) and MT1-MMP$^{-/-}$ mice (n = 2). Errors in bar graphs are SEM; $^*P < .05$, $^{**}P < .01$.

## Discussion

In this report, we identified MT1-MMP as a key player of postnatal hematopoiesis. We demonstrate that MT1-MMP–expressing cells serve as key links between the HIF-1 regulatory system and transcriptional regulation of vital niche chemokines/cytokines necessary for HSC maintenance and cell differentiation (Figure 7). Specifically, we show that MT1-MMP deficiency leads to impairment of steady-state hematopoiesis because of a reduced HSC pool and a trilineage differentiation block. Mechanistically, we provide evidence that MT1-MMP deficiency in niche/stromal cells increases cytosolic FIH1 on expense of the membrane-associated FIH1 expression, thereby preventing transcription of the HIF-responsive genes EPO, KitL, IL-7, and SDF-1α. Thus, this study identifies MT1-MMP as a key molecular link between hypoxia and the regulation of vital HSC niche factors.

We reported that MMP-9 and plasminogen activation is important for the ectodomain shedding of the hematopoietic growth factor like KitL.[10,19] MT1-MMP can activate various proteases, including plasminogen or MMP-2, which in turn can activate MMP-9. It has been reported that MMP-2 activation can process

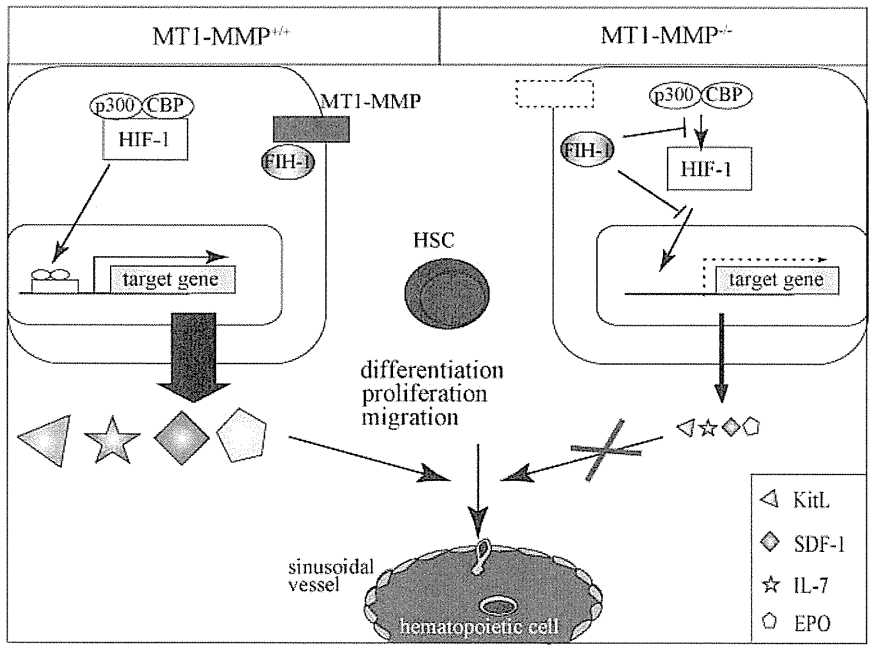


**Figure 7. Proposed model of the role of MT1-MMP–expressing niche cells, which serve as key links between the HIF-1 regulatory system and transcriptional regulation of vital niche chemokines/cytokines necessary for HSC maintenance and cell differentiation.** MT1-MMP deficiency in niche cells up-regulates FIH1 expression, thereby preventing transcription of the HIF-responsive genes *EPO*, *KitL*, *IL-7*, and *SDF-1α*. MT1-MMP deficiency leads to impaired steady-state hematopoiesis because of a trilineage differentiation block.

SDF-1/CXCL12.[40] We are currently examining whether ectodomain shedding by MT1-MMP–activated MMPs could be another reason for the low cytokine levels observed in MT1-MMP$^{-/-}$ mice.

Other known modulators of the BM and of niches such as the cancer stem cell niche, including vascular endothelial growth factor-A, angiopoietin 2, placental growth factor, and platelet-derived growth factor B, are also HIF-regulated target genes and therefore might also depend on MT1-MMP function.[7,8,41-43] But further studies will be needed to proof this concept.

Using BM chimeras generated using MT1-MMP$^{-/-}$ and MT1-MMP$^{+/+}$ donor cells, we showed that the developmental T-cell differentiation arrest observed in MT1-MMP$^{-/-}$ mice was mainly because of a niche defect, and not because of the impaired stem cell pool observed in these mice. In MT1-MMP$^{-/-}$ mice, we found preferential differentiation into CD4 SP thymocytes, which is most likely because of impaired Notch signaling.[44] Indeed, a recent study demonstrated that MT1-MMP directly cleaves Dll-1, a Notch ligand on BM stromal cells.[45] The continued presence of Dll-1 is required for T-cell commitment and maintenance at the DN1 and DN2 stages of thymocyte development. In the absence of Notch signaling, the developing DN1 and DN2 thymocytes adopt a NK-cell fate by default, a phenomena that we indeed observed in the MT1-MMP$^{-/-}$ mice.[46]

IL-7 signaling and Notch signaling are implicated in B-cell lymphopoiesis.[47] We found that HSC differentiation toward B lymphocytes was compromised in MT1-MMP–deficient BM cells. The long-term proliferation capacity of BM pre-B1 cells is known to be critically dependent on KitL and IL-7 expression and signaling, factors that we have shown require the presence of MT1-MMP for their expression.[48,49] Furthermore, we provide evidence that MT1-MMP deficiency in stromal cells also impairs the expression of SDF-1α, which is a key regulator of B-cell lymphopoiesis and BM myelopoiesis.[50] Our data are consistent with those of a previous report, which observed that defects in B lymphopoiesis are modulated by MT1-MMP–mediated cleavage of Dll-1 on BM stromal cells.[45] Impaired BM myelopoiesis was found in MT1-MMP–deficient mice, regardless of the fact that G-CSF expression was normal. Factors such as KitL and SDF-1α have also been implicated in myelopoiesis, and therefore might be at least partially responsible for the observed phenotype.

In addition, in vivo administration of KitL and SDF-1α rescued the pancytopenia in MT1-MMP–deficient mice. As both growth factors can increase the egress and mobilization of mature hematopoietic cells, but also can promote hematopoietic cell differentiation, the restoration of PB counts in MT1-MMP–deficient mice could be because of improved hematopoietic cell migration and/or differentiation. We confirmed data by Vagima et al demonstrating that MT1-MMP is expressed on hematopoietic progenitor cells.[21] This group showed that MT1-MMP is required for G-CSF–mediated hematopoietic progenitor cell mobilization.

SDF-1α is required for the maintenance of BM HSCs and is expressed by both perivascular and endosteal cells.[11,13] Deficits in the maintenance of the HSC pool in the absence of CXCR4 are HSC autonomous. Indeed, we could show that MT1-MMP deficiency altered SDF-1α/CXCL12-CXCR4 signaling and impaired the stem cell pool.

Our studies on the role of MT1-MMP in hematopoietic niche/stromal cells provide the rationale for further exploration of MT1-MMP in other hypoxic niches, for example, the cancer niche or the "ischemia-associated niche," as MT1-MMP seems to control the hematopoietic cell response in those diseases by controlling cytokine production.

## Acknowledgments

The authors thank the FACS core facility in the Institute of Medical Science (University of Tokyo) for their help. They also thank Dr Hideo Ema for critical advice. Stephanie C. Napier kindly provided editorial assistance to the authors during the preparation of this manuscript. Pauline O'Grady edited the manuscript.

This work was supported by grants from the Japan Society for the Promotion of Science and Grants-in-Aid for Scientific Research from the Ministry of Education, Culture, Sports, Science and Technology (MEXT; K.H. and B.H.); a Grant-in-Aid for Scientific Research on Priority Areas from the MEXT (K.H.); the Mitsubishi Pharma Research Foundation (K.H.); a Grant-in-Aid for Scientific Research on Innovative Areas from the MEXT (B.H.); and the Program for Improvement of the Research Environment for Young Researchers (B.H.) funded by the Special Coordination Funds for Promoting Science and Technology of the MEXT, Japan. In addition, this work was supported by grants from ENSHIN Medical Research Foundation, from Kyowa Hakko Kirin Co Ltd, and from Daiichi Sankyo Company Ltd (K.H.).

## Authorship

Contribution: C.N., B.H., and K.H. designed and performed experiments, analyzed and interpreted data, and wrote the manuscript; K.K., Y.T., I.G., A.S., M.O.-K., Y.M., M.N., T.S., N.K., T.K., and S.K.-K. participated in performing experiments, data analysis, and discussion; M.S. and H.N. interpreted data; and H.N., B.H., and K.H. assisted with experimental design and manuscript writing.

Conflict-of-interest disclosure: The authors declare no competing financial interests.

Correspondence: Koichi Hattori, MD, PhD, Center for Stem Cell Biology and Regenerative Medicine, Institute of Medical Science at the University of Tokyo, 4-6-1, Shirokanedai, Minato-ku, Tokyo 108-8639, Japan; e-mail: khattori@ims.u-tokyo.ac.jp.

## References

1. Schofield R. The relationship between the spleen colony-forming cell and the haemopoietic stem cell. *Blood Cells.* 1978;4(1-2):7-25.
2. Adams GB, Chabner KT, Alley IR, et al. Stem cell engraftment at the endosteal niche is specified by the calcium-sensing receptor. *Nature.* 2006; 439(7076):599-603.
3. Takubo K, Goda N, Yamada W, et al. Regulation of the HIF-1alpha level is essential for hematopoietic stem cells. *Cell Stem Cell.* 2010;7(3):391-402.
4. Jang YY, Sharkis SJ. A low level of reactive oxygen species selects for primitive hematopoietic stem cells that may reside in the low-oxygenic niche. *Blood.* 2007;110(8):3056-3063.
5. Adelman DM, Maltepe E, Simon MC. Multilineage embryonic hematopoiesis requires hypoxic ARNT activity. *Genes Dev.* 1999;13(19):2478-2483.
6. Scortegagna M, Morris MA, Oktay Y, Bennett M, Garcia JA. The HIF family member EPAS1/HIF-2alpha is required for normal hematopoiesis in mice. *Blood.* 2003;102(5):1634-1640.
7. Rey S, Semenza GL. Hypoxia-inducible factor-1-dependent mechanisms of vascularization and vascular remodelling. *Cardiovasc Res.* 2010; 86(2):236-242.
8. Hattori K, Heissig B, Wu Y, et al. Placental growth factor reconstitutes hematopoiesis by recruiting VEGFR1(+) stem cells from bone-marrow microenvironment. *Nat Med.* 2002;8(8):841-849.
9. Arai F, Hirao A, Ohmura M, et al. Tie2/angiopoietin-1 signaling regulates hematopoietic stem cell quiescence in the bone marrow niche. *Cell.* 2004; 118(2):149-161.
10. Heissig B, Hattori K, Dias S, et al. Recruitment of stem and progenitor cells from the bone marrow

niche requires MMP-9 mediated release of kit-ligand. *Cell.* 2002;109(5):625-637.

11. Kollet O, Dar A, Shivtiel S, et al. Osteoclasts degrade endosteal components and promote mobilization of hematopoietic progenitor cells. *Nat Med.* 2006;12(6):657-664.
12. Ehninger A, Trumpp A. The bone marrow stem cell niche grows up: mesenchymal stem cells and macrophages move in. *J Exp Med.* 2011;208(3): 421-428.
13. Sugiyama T, Kohara H, Noda M, Nagasawa T. Maintenance of the hematopoietic stem cell pool by CXCL12-CXCR4 chemokine signaling in bone marrow stromal cell niches. *Immunity.* 2006; 25(6):977-988.
14. Tokoyoda K, Egawa T, Sugiyama T, Choi BI, Nagasawa T. Cellular niches controlling B lymphocyte behavior within bone marrow during development. *Immunity.* 2004;20(6):707-718.
15. Egawa T, Kawabata K, Kawamoto H, et al. The earliest stages of B cell development require a chemokine stromal cell-derived factor/pre-B cell growth-stimulating factor. *Immunity.* 2001;15(2): 323-334.
16. Fleming HE, Paige CJ. Pre-B cell receptor signaling mediates selective response to IL-7 at the pro-B to pre-B cell transition via an ERK/MAP kinase-dependent pathway. *Immunity.* 2001; 15(4):521-531.
17. Peschon JJ, Morrissey PJ, Grabstein KH, et al. Early lymphocyte expansion is severely impaired in interleukin 7 receptor-deficient mice. *J Exp Med.* 1994;180(5):1955-1960.
18. von Freeden-Jeffry U, Vieira P, Lucian LA, McNeil T, Burdach SE, Murray R. Lymphopenia in interleukin (IL)-7 gene-deleted mice identifies IL-7 as a nonredundant cytokine. *J Exp Med.* 1995; 181(4):1519-1526.
19. Heissig B, Lund LR, Akiyama H, et al. The plasminogen fibrinolytic pathway is required for hematopoietic regeneration. *Cell Stem Cell.* 2007; 1(6):658-670.
20. Lehti K, Rose NF, Valavaara S, Weiss SJ, Keski-Oja J. MT1-MMP promotes vascular smooth muscle dedifferentiation through LRP1 processing. *J Cell Sci.* 2009;122:126-135.
21. Vagima Y, Avigdor A, Goichberg P, et al. MT1-MMP and RECK are involved in human CD34+ progenitor cell retention, egress, and mobilization. *J Clin Invest.* 2009;119(3):492-503.
22. Chun TH, Hotary KB, Sabeh F, Saltiel AR, Allen ED, Weiss SJ. A pericellular collagenase directs the 3-dimensional development of white adipose tissue. *Cell.* 2006;125(3):577-591.
23. Sakamoto T, Seiki M. A membrane protease regulates energy production in macrophages by activating hypoxia-inducible factor-1 via a non-proteolytic mechanism. *J Biol Chem.* 2010; 285(39):29951-29964.
24. Sakamoto T, Seiki M. Cytoplasmic tail of MT1-MMP regulates macrophage motility independently from its protease activity. *Genes Cells.* 2009;14(5):617-626.
25. Itoh Y, Seiki M. MT1-MMP: a potent modifier of pericellular microenvironment. *J Cell Physiol.* 2006;206(1):1-8.
26. Hotary KB, Allen ED, Brooks PC, Datta NS, Long MW, Weiss SJ. Membrane type I matrix metalloproteinase usurps tumor growth control imposed by the three-dimensional extracellular matrix. *Cell.* 2003;114(1):33-45.
27. Seiki M. Membrane-type 1 matrix metalloproteinase: a key enzyme for tumor invasion. *Cancer Lett.* 2003;194(1):1-11.
28. Holmbeck K, Bianco P, Caterina J, et al. MT1-MMP-deficient mice develop dwarfism, osteopenia, arthritis, and connective tissue disease due to inadequate collagen turnover. *Cell.* 1999;99(1): 81-92.
29. Hattori K, Heissig B, Tashiro K, et al. Plasma elevation of stromal cell-derived factor-1 induces mobilization of mature and immature hematopoietic progenitor and stem cells. *Blood.* 2001; 97(11):3354-3360.
30. Taniwaki K, Fukamachi H, Komori K, et al. Stroma-derived matrix metalloproteinase (MMP)-2 promotes membrane type 1-MMP-dependent tumor growth in mice. *Cancer Res.* 2007;67(9):4311-4319.
31. Mendez-Ferrer S, Michurina TV, Ferraro F, et al. Mesenchymal and haematopoietic stem cells form a unique bone marrow niche. *Nature.* 2010; 466(7308):829-834.
32. Maiese K, Chong ZZ, Shang YC. Raves and risks for erythropoietin. *Cytokine Growth Factor Rev.* 2008;19(2):145-155.
33. Munugalavadla V, Kapur R. Role of c-Kit and erythropoietin receptor in erythropoiesis. *Crit Rev Oncol Hematol.* 2005;54(1):63-75.
34. Wang W, Horner DN, Chen WL, Zandstra PW, Audet J. Synergy between erythropoietin and stem cell factor during erythropoiesis can be quantitatively described without co-signaling effects. *Biotechnol Bioeng.* 2008;99(5):1261-1272.
35. Socolovsky M, Nam H, Fleming MD, Haase VH, Brugnara C, Lodish HF. Ineffective erythropoiesis in Stat5a(−/−)5b(−/−) mice due to decreased survival of early erythroblasts. *Blood.* 2001; 98(12):3261-3273.
36. Link A, Vogt TK, Favre S, et al. Fibroblastic reticular cells in lymph nodes regulate the homeostasis of naive T cells. *Nat Immunol.* 2007;8(11):1255-1265.
37. Webb JD, Coleman ML, Pugh CW. Hypoxia, hypoxia-inducible factors (HIF), HIF hydroxylases and oxygen sensing. *Cell Mol Life Sci.* 2009; 66(22):3539-3554.
38. Mahon PC, Hirota K, Semenza GL. FIH-1: a novel protein that interacts with HIF-1alpha and VHL to mediate repression of HIF-1 transcriptional activity. *Genes Dev.* 2001;15(20):2675-2686.
39. Kasper LH, Boussouar F, Boyd K, et al. Two transactivation mechanisms cooperate for the bulk of HIF-1-responsive gene expression. *EMBO J.* 2005;24(22):3846-3858.
40. McQuibban GA, Butler GS, Gong JH, et al. Matrix metalloproteinase activity inactivates the CXC chemokine stromal cell-derived factor-1. *J Biol Chem.* 2001;276(47):43503-43508.
41. Ceradini DJ, Kulkarni AR, Callaghan MJ, et al. Progenitor cell trafficking is regulated by hypoxic gradients through HIF-1 induction of SDF-1. *Nat Med.* 2004;10(8):858-864.
42. Forsythe JA. Activation of vascular endothelial growth factor gene transcription by hypoxia-inducible factor 1. *Mol Cell Biol.* 1996;16(9):4604-4613.
43. Simon MP, Tournaire R, Pouyssegur J. The angiopoietin-2 gene of endothelial cells is up-regulated in hypoxia by a HIF binding site located in its first intron and by the central factors GATA-2 and Ets-1. *J Cell Physiol.* 2008;217(3): 809-818.
44. Robey E, Chang D, Itano A, et al. An activated form of notch influences the choice between CD4 and CD8 T cell lineages. *Cell.* 1996;87(3):483-492.
45. Jin G, Zhang F, Chan KM, et al. MT1-MMP cleaves Dll1 to negatively regulate Notch signalling to maintain normal B-cell development. *EMBO J.* 2011;30:2281-2293.
46. Schmitt TM, Ciofani M, Petrie HT, Zuniga-Pflucker JC. Maintenance of T cell specification and differentiation requires recurrent notch receptor-ligand interactions. *J Exp Med.* 2004;200(4): 469-479.
47. Namen AE, Lupton S, Hjerrild K, et al. Stimulation of B-cell progenitors by cloned murine interleukin-7. *Nature.* 1988;333(6173):571-573.
48. Rolink A, Streb M, Nishikawa S, Melchers F. The c-kit-encoded tyrosine kinase regulates the proliferation of early pre-B cells. *Eur J Immunol.* 1991; 21(10):2609-2612.
49. Sudo T, Nishikawa S, Ohno N, Akiyama N, Tamakoshi M, Yoshida H. Expression and function of the interleukin 7 receptor in murine lymphocytes. *Proc Natl Acad Sci U S A.* 1993;90(19): 9125-9129.
50. Nagasawa T, Hirota S, Tachibana K, et al. Defects of B-cell lymphopoiesis and bone-marrow myelopoiesis in mice lacking the CXC chemokine PBSF/SDF-1. *Nature.* 1996;382(6592):635-638.

# Induced pluripotent stem cells from CINCA syndrome patients as a model for dissecting somatic mosaicism and drug discovery

Takayuki Tanaka,[1] Kazutoshi Takahashi,[1] Mayu Yamane,[1] Shota Tomida,[1] Saori Nakamura,[1] Koichi Oshima,[1] Akira Niwa,[1] Ryuta Nishikomori,[2] Naotomo Kambe,[3] Hideki Hara,[4] Masao Mitsuyama,[4] Nobuhiro Morone,[5] John E. Heuser,[5] Takuya Yamamoto,[1] Akira Watanabe,[1] Aiko Sato-Otsubo,[6] Seishi Ogawa,[6] Isao Asaka,[1] Toshio Heike,[2] Shinya Yamanaka,[1,5,7,8] Tatsutoshi Nakahata,[1,2] and Megumu K. Saito[1]

[1]Center for iPS Cell Research and Application and [2]Department of Pediatrics, Kyoto University, Kyoto, Japan; [3]Department of Dermatology, Chiba University Graduate School of Medicine, Chiba, Japan; [4]Department of Microbiology and [5]Institute for Integrated Cell-Material Sciences, Kyoto University, Kyoto, Japan; [6]Cancer Genomics Project, University of Tokyo, Tokyo, Japan; [7]Yamanaka iPS Cell Special Project, Japan Science and Technology Agency, Kawaguchi, Japan; and [8]Gladstone Institute of Cardiovascular Disease, San Francisco, CA

**Chronic infantile neurologic cutaneous and articular (CINCA) syndrome is an IL-1–driven autoinflammatory disorder caused mainly by *NLRP3* mutations. The pathogenesis of CINCA syndrome patients who carry *NLRP3* mutations as somatic mosaicism has not been precisely described because of the difficulty in separating individual cells based on the presence or absence of the mutation. Here we report the generation of *NLRP3*-mutant and nonmutant-induced pluripotent stem cell (iPSC) lines from 2 CINCA syndrome patients with somatic mosaicism, and describe their differentiation into macrophages (iPS-MPs). We found that mutant cells are predominantly responsible for the pathogenesis in these mosaic patients because only mutant iPS-MPs showed the disease relevant phenotype of abnormal IL-1β secretion. We also confirmed that the existing anti-inflammatory compounds inhibited the abnormal IL-1β secretion, indicating that mutant iPS-MPs are applicable for drug screening for CINCA syndrome and other NLRP3-related inflammatory conditions. Our results illustrate that patient-derived iPSCs are useful for dissecting somatic mosaicism and that *NLRP3*-mutant iPSCs can provide a valuable platform for drug discovery for multiple NLRP3-related disorders. (*Blood.* 2012;120(6):1299-1308)**

## Introduction

Chronic infantile neurologic cutaneous and articular syndrome (CINCA syndrome; MIM #607715) is a dominantly inherited autoinflammatory disease characterized by systemic inflammation with an urticaria-like rash, neurologic manifestations, and arthropathy.[1] *NLRP3* mutation is the first and so far the only identified mutation that is responsible for CINCA syndrome.[2,3] *NLRP3* is expressed mainly in myelomonocytic lineage cells and chondrocytes[3] and acts as an intracellular sensor of danger signals from various cellular insults. In normal macrophages, a first stimulus, such as lipopolysaccharide (LPS), induces the synthesis of NLRP3 and the biologically inactive proIL-1β.[4] A second stimulus, such as ATP, enhances the assembly of a protein complex called the NLRP3-inflammasome.[5] The inflammasome contains caspase1, which executes the proteolytic maturation and secretion of IL-1β. Although normal monocytes/macrophages show no or limited IL-1β secretion in response to LPS stimulation alone, CINCA patients' cells exhibit robust IL-1β secretion because the mutant NLRP3-inflammasome is autoactivated without the need for any second stimulus.[6] It is therefore thought that the manifestations of CINCA syndrome are predominantly caused by the excessive secretion of the proinflammatory cytokine, IL-1β, and this concept is supported by the efficacy of an IL-1 receptor antagonist (IL-1Ra) for decreasing most of the symptoms.[7] However, because IL-1Ra treatment does not seem to ameliorate the characteristic arthropathy of cartilage overgrowth and joint contraction,[8] a more specific therapeutic approach that directly modulates the NLRP3-inflammasome is desired.

Although approximately half of CINCA patients carry heterozygous gain-of-function mutations of the *NLRP3* gene,[2,3] 30% to 40% of all patients have mutations in *NLRP3* in only a small number of somatic cells.[9,10] Because the population of mutant cells is relatively small (4.2%-35.8% in blood cells), it remains controversial whether the small fraction of *NLRP3*-mutated cells actually causes the strong autoinflammation observed in CINCA patients, or whether the *NLRP3* mutations found in mosaic patients are just a bystander, with all cells carrying an unknown mutation of another gene that causes the disease.[11]

Somatic mosaicism refers to the presence of more than 1 genetically distinct cell population in a single person, and has been identified in patients with various diseases.[12,13] The relevance of somatic mosaicism to the onset of diseases has been suggested mainly through sequence-based approaches. However, direct evidence that a cell population with a distinct genetic property shows disease-specific characteristics is lacking because it has been impossible to separately extract individual live cells from affected tissues to assess their biologic characteristics. Regarding hematopoietic disorders in which mutant cells show decreased expression of a certain protein, genetic heterogeneity caused by somatic mutations was detected by flow cytometry after intracellular staining,[14-16] but sorting out alive mutant and nonmutant cells for evaluating biologic property has been impossible.

Submitted March 27, 2012; accepted May 29, 2012. Prepublished online as *Blood* First Edition paper, June 21, 2012; DOI 10.1182/blood-2012-03-417881.

The online version of this article contains a data supplement.

The publication costs of this article were defrayed in part by page charge payment. Therefore, and solely to indicate this fact, this article is hereby marked "advertisement" in accordance with 18 USC section 1734.